Supporting Information:

# Triggered Gate Opening and Breathing Effects during Selective $CO_2$ Adsorption by Merlinoite Zeolite

Veselina M. Georgieva,[1] Elliott L. Bruce,[1] Maarten C. Verbraeken,[2] Aaron R. Scott,[3] William J. Casteel, Jr.,[3] Stefano Brandani[2] and Paul A. Wright[1,*]

*[1] EaStCHEM School of Chemistry, University of St Andrews, Purdie Building, North Haugh, St Andrews, UK; [2] School of Engineering, University of Edinburgh, The King's Buildings, Edinburgh, UK; [3] Air Products and Chemicals Inc., 7201 Hamilton Blvd., Allentown, PA18195 USA*

**Contents**

## S1. Synthesis and Initial Characterisation

### Synthesis

Colloidal silica, Ludox HS-40 (12.5 g; 40%, suspension in water; Sigma-Aldrich) was added to 35% aqueous solution of tetraethylammonium hydroxide (3.15 g; 35% TEOAH, Sigma-Aldrich) and the resulting mixture was stirred for 1 h. To this mixture, a solution made by dissolving metal Al (0.8 g, 99%, Alfa Aesar) in 3 g TEAOH and KOH (0.6 g, 85%, Fisher Chemicals), which was also mixed for 1 h, was added. The gel formed was continuously stirred for 10 min, transferred to a PTFE-lined stainless-steel autoclave and hydrothermally treated at 423 K under slow rotation (60 rpm). The resultant solid product, collected after 96 h, was filtered and washed with distilled water until the pH value of the filtrate was about 8. After washing, all samples were dried at 343 K for 12 h.

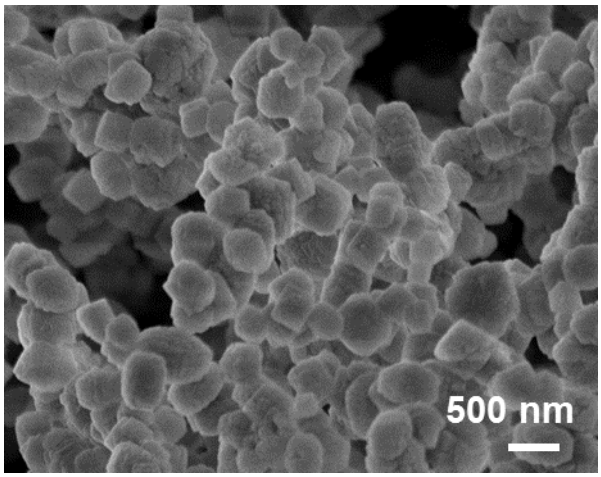


Figure S1.1. SEM micrographs of K,TEA-MER zeolite sample.

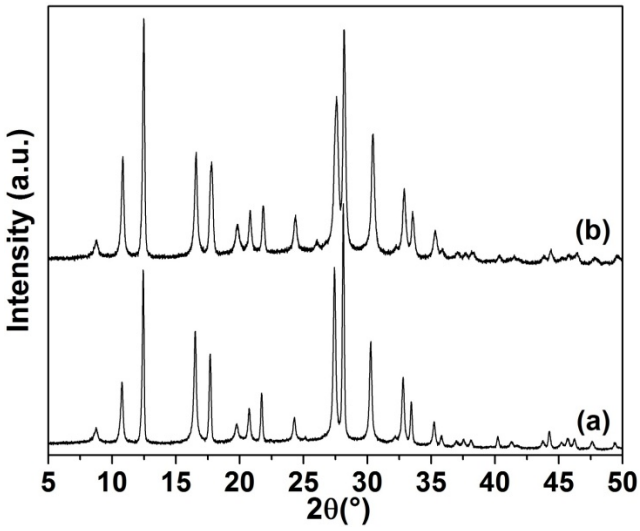


Figure S1.2. PXRD patterns of hydrated, as-prepared (a) K,TEA-MER and calcined (b) K,H-MER

**Solid-State NMR Details**

Solid-state NMR spectra were recorded using a Bruker Avance III spectrometer equipped with a 9.4 T wide-bore superconducting magnet (Larmor frequencies of 104.3 and 79.5 MHz, respectively for $^{27}$Al and $^{29}$Si). Samples were packed into zirconia MAS rotors with outer diameters of 4 mm and rotated at MAS rates of up to 14 kHz using a standard Bruker MAS probe. $^{27}$Al NMR spectra were acquired using a short pulse of 0.5 μs (inherent flip angle of ~12°), with signal averaging for 128-1024 transients and a recycle interval of 0.5 s. Chemical shifts are reported in ppm relative to 0.1 M $Al(NO_3)_3$ using $Al(acac)_3$ as a secondary solid reference ($\delta_{iso}$ = 0.0 ppm). $^{29}$Si NMR spectra were acquired using a π/2 pulse of 2.75 μs, with signal averaging for 128 - 512 transients with a recycle interval of 120 s. Chemical shifts are reported in ppm relative to TMS using forsterite ($Mg_2SiO_4$) as a secondary solid reference ($\delta_{iso}$ = –62 ppm). Deconvolution of the $^{29}$Si MAS NMR of the as-prepared K,TEA-MER, in which all aluminium occupies tetrahedral sites and all tetrahedral sites are crystallographically equivalent, was used to determine the framework Si/Al ratio of zeolite MER and used to calibrate the Si/Al ratios determined via EDX.

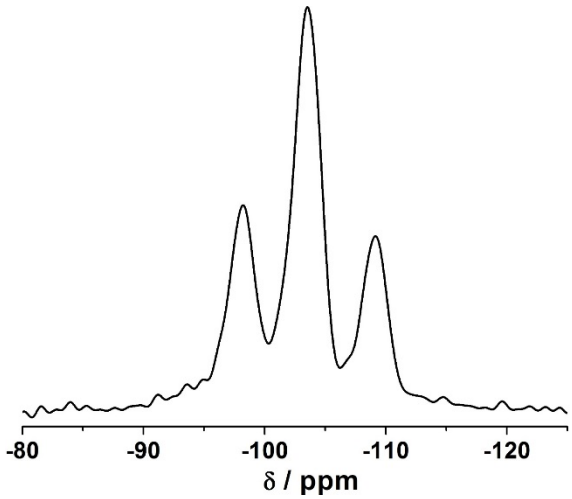


Figure S1.3. $^{29}$Si MAS NMR spectra of as-prepared K,TEA-MER.

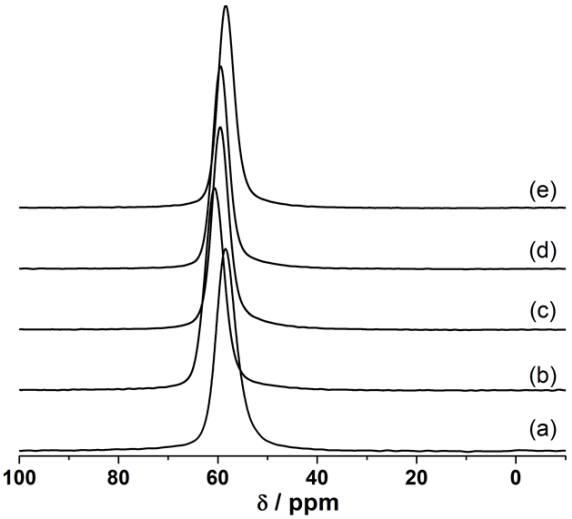


Figure S1.4. $^{27}$Al MAS NMR spectra of (a) K,TEA-MER, (b) K,H-MER, (c) Na-MER, (d) K-MER and (e) Cs-MER.

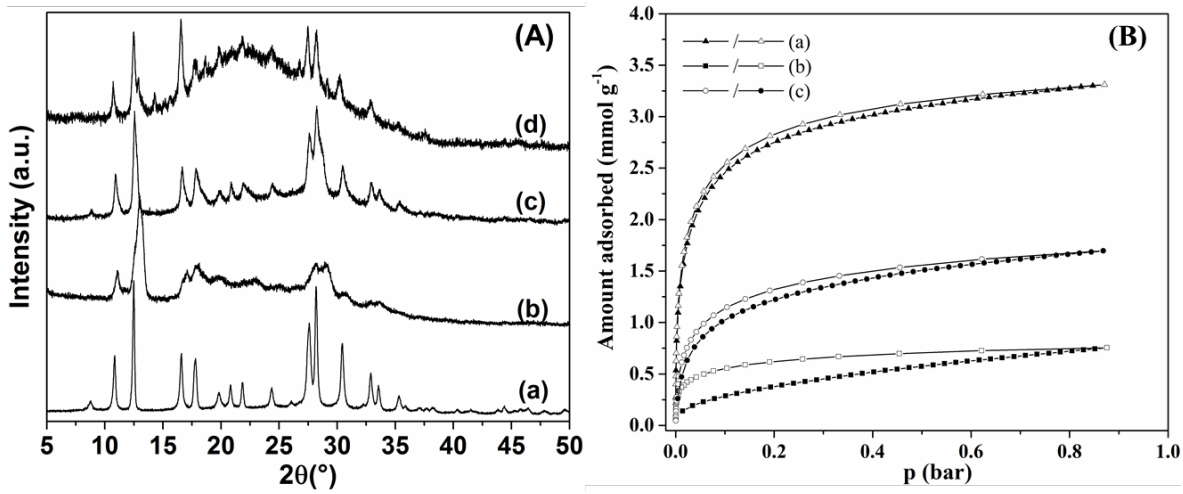


Figure S1.5. A) PXRD patterns of hydrated (a) K-MER, (b) Li-MER, (c) re-exchanged Li-MER and (d) H-MER; (B) $CO_2$ adsorption (closed symbols), desorption (open symbols) isotherms at 298 K for (a) K-MER (triangles), (b) Li-MER (squares) and (c) re-exchanged Li-MER (circles).

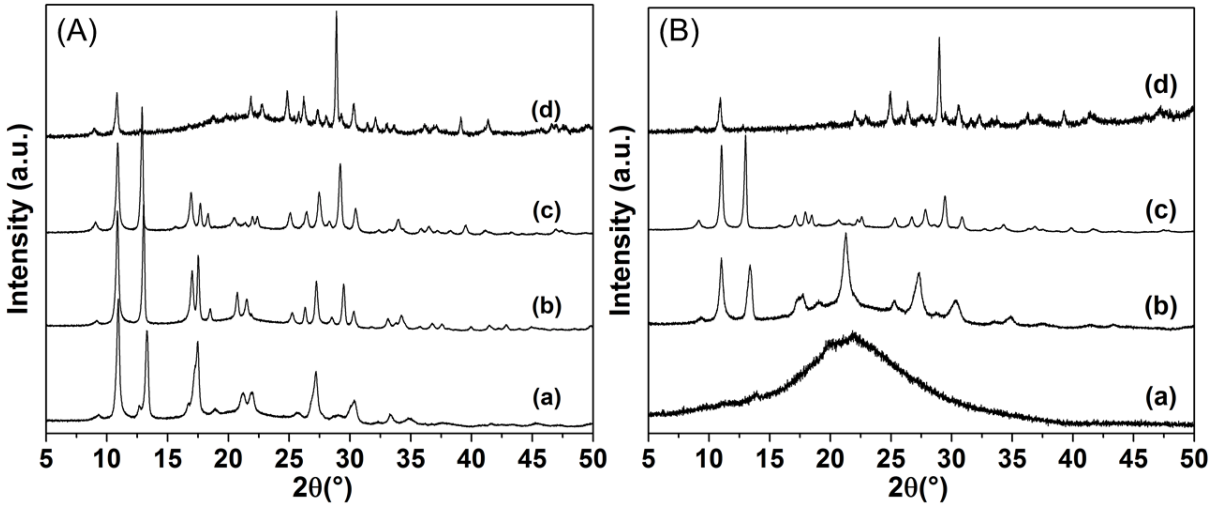


Figure S1.6. PXRD patterns of dehydrated, as-prepared (A) (a) Li,TEA-MER, (b) Na,TEA-MER, (c) K,TEA-MER, (d) Cs, TEA-MER and calcined (B) (a) Li,H-MER, (b) Na,H-MER, (c) K,H-MER, (d) Cs,H-MER. All patterns collected at 298 K using the same operating conditions.

Table S1.1. Literature reports of merlinoite structures

| Ref | Sample | Si/Al | Cations | Space group | Hydrated? | Fit? | $T_{collection}$ (K) | a* | b* | c* |
|---|---|---|---|---|---|---|---|---|---|---|
| Galli [1] | Natural from Cupaello | 2.45 | K,Ca,Ba,Na | *Immm* | H | - | - | 14.116 | 14.229 | 9.946 |
| Skofteland [2] | KOH-MER | 1.8 | $K_{11.5}$ | *Immm* | H | y | 298 | 14.0716(6) | 14.1978(5) | 10.02912(34) |
| Skofteland [2] | KOH-MER | 1.8 | $K_{11.5}$ | *Pnnm* | D | n | 298 | 13.416(6) | 13.4118(5) | 9.79696(22) |
| Skofteland [2] | $KNO_3$-MER | 2.4 | $K_{9.5}$ | *Pnnm* | H | n | 298 | - | - | - |
| Pakhomova [3] | Natural from Khibiny masif | 1.7 | $K_{10}Na_1$ | *Immm* | H | n | 298 | 14.0312(5) | 14.2675(6) | 10.0874(4) |
| Pakhomova [3] | Natural from Khibiny masif | 1.7 | $K_{10}Na_1$ | $P4_2/nmc$ | D | n | 498 | 13.341(4) | 13.341(4) | 9.707(4) |
| Bieniok [4] | Synthetic W | 2.1 | $K_{10.3}$ | *Immm* | H | y | 298 | 14.0948(6) | 14.2026(6) | 10.0421(5) |
| Barrett [5] | MER | 3.8 | $K_{5.2}TEA_{0.8}H_{0.7}$ | *Immm* | H | y | 298 | 14.1291(10) | 14.1308(10) | 9.9274(5) |
| Yakubovich, [6] | MER | 1.67 | $K_{7.28}Na_{4.72}$ | *Immm* | H | - | - | 13.863 | 14.135 | 10.047 |

Table S1.2. Literature reports of cation site occupancies in merlinoite samples

| Sample | Space Group | I | | Ia | | II | | IIa | | IIb | | III | |
|---|---|---|---|---|---|---|---|---|---|---|---|---|---|
| | | occ | tot | occ | tot | occ | tot | occ | tot | occ | tot | occ | tot |
| Galli [1], natural | *Immm* | 0 | 0 | 0 | 0 | - | - | 0.42 | 1.68 | 0.41 | 1.64 | 0 | 0 |
| Skofteland[2] KOH-MER H | *Immm* | 0.7 | 2.8 | 0 | 0 | - | - | 1 | 4 | 1 | 4 | 0.15 | 0.6 |
| Skofteland[2] KOH-MER DH | *Pnmm* | 0 | 0 | 1 | 2 | - | - | 1 | 4 | 0.75 | 6 | 0 | 0 |
| Pakhomova[3] H | *Immm* | 0.627 | 5 | 0 | 0 | - | - | 1 | 4 | 0.59 | 2.36 | 0 | 0 |
| Pakhomova[3] DH | $P4_2/nmc$ | 0.073 | 0.292 | 0.95 | 1.9 | 0.796 | 6.368 | - | - | - | - | 0.627 | 2.51 |

## S2. Results of refinement of hydrated merlinoite in this work

Table S2.1. Crystallography of hydrated Na-, K- (and K, H-) and Cs-MER in this work

| Sample | Na-MER | K-MER | K,H-MER | Cs-MER |
|---|---|---|---|---|
| **Unit Cell** | $Na_{7.4}Si_{32}O_{64}.O_{20.0}$ | $K_{6.6}Si_{32}O_{64}.O_{18.5}$ | $K_{6.9}Si_{32}O_{64}.O_{19.4}$ | $Cs_{7.1}Si_{32}O_{64}.O_{12.9}$ |
| **T (K)** | 298 | 298 | 298 | 298 |
| **Space Group** | *Immm* | $P4_2/nmc$ | $P4_2/nmc$ | $P4_2/nmc$ |
| **X-ray Source** | Stoe | Stoe | Stoe | PANALYTICAL |
| **λ (Å)** | 1.54056 | 1.54056 | 1.54056 | 1.54056 |
| **a (Å)** | 14.144(2) | 14.114(1) | 14.136(1) | 14.219(1) |
| **b (Å)** | 14.141(2) | - | - | - |
| **c (Å)** | 10.022(1) | 9.916(1) | 9.930(1) | 10.015(1) |
| **V (Å$^3$)** | 2005(1) | 1975(1) | 1984(1) | 2025(1) |
| $R_p$ | 7.3% | 7.3% | 5.6% | 6.2% |
| $R_{wp}$ | 9.4% | 9.2% | 7.2% | 8.0% |
| $\chi^2$ | 2.2 | 1.5 | 1.8 | 1.8 |

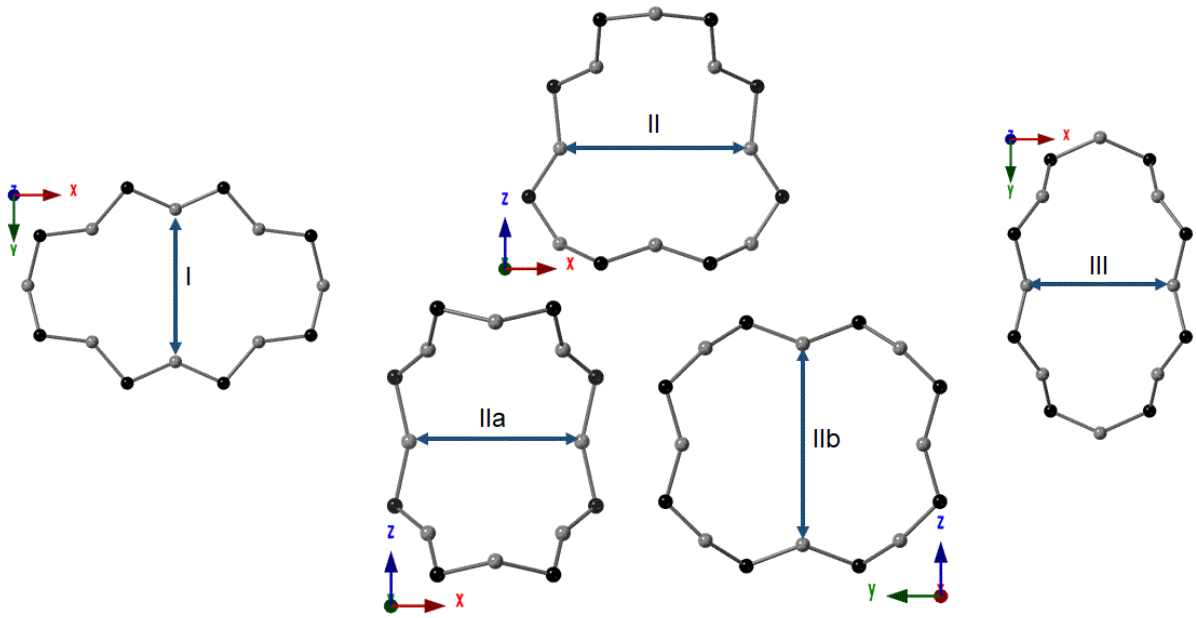


Figure S2.1 Estimation of the free diameter of windows of type I, II and III, as described in the text. The O-O distances were taken from the crystallographic structure, and twice the van der Waals radius of O, 2 × 1.35 Å. was subtracted to give the reported free diameters.

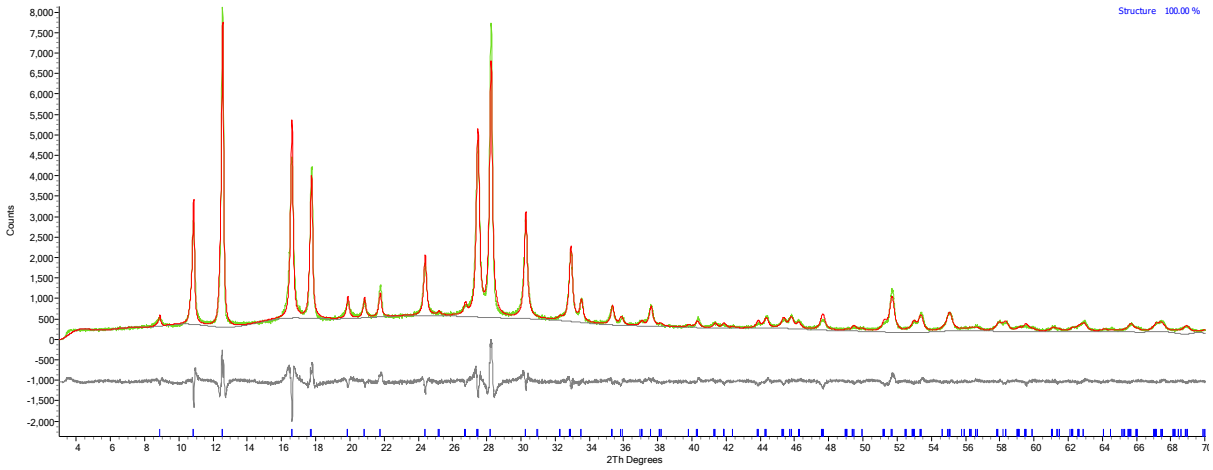


Figure S2.2. Rietveld fit for hydrated Na-MER

Table S2.2. Refined structure of hydrated Na-MER

| Site | Type | x | y | z | Occ | Mult | Biso |
|---|---|---|---|---|---|---|---|
| **Na1** | Na | 0 | 1 | 0.805(15) | 0.38(13) | 4 | 2 |
| **Na2** | Na | 0.5 | 0.718(2) | 1 | 0.95(5) | 4 | 2 |
| **Na3** | Na | 0 | 0.5 | 0.711(16) | 0.36(3) | 4 | 2 |
| **Ow1** | O | 0 | 1 | 0.725(10) | 0.97(17) | 4 | 2 |
| **Ow2** | O | 0.5 | 0 | 0 | 1.00(8) | 2 | 2 |
| **Ow3** | O | 0.5 | 0.5 | 0.5 | 0.94(5) | 2 | 2 |
| **Ow4** | O | 0.301(3) | 0.385(2) | 0 | 0.96(3) | 8 | 2 |
| **Ow5** | O | 0.428(3) | 0.377(3) | 0 | 0.64(4) | 8 | 2 |
| **O1** | O | 0.160(2) | 0.1598(19) | 0.2088(17) | 1 | 16 | 1 |
| **O2** | O | 0.112(3) | 0.290(3) | 0 | 1 | 8 | 1 |
| **O5** | O | 0.707(3) | 0.1276(19) | 0 | 1 | 8 | 1 |
| **O3** | O | 0 | 0.247(2) | 0.198(2) | 1 | 8 | 1 |
| **O6** | O | 0.757(2) | 0 | 0.178(3) | 1 | 8 | 1 |
| **O4** | O | 0.1502(16) | 0.3543(15) | 0.244(3) | 1 | 16 | 1 |
| **Si1** | Si | 0.1107(10) | 0.2582(11) | 0.1499(11) | 0.8 | 16 | 1 |
| **Al1** | Al | 0.1107(10) | 0.2582(11) | 0.1499(11) | 0.2 | 16 | 1 |
| **Si2** | Si | 0.7377(11) | 0.1026(11) | 0.1706(10) | 0.8 | 16 | 1 |
| **Al2** | Al | 0.7377(11) | 0.1026(11) | 0.1706(10) | 0.2 | 16 | 1 |

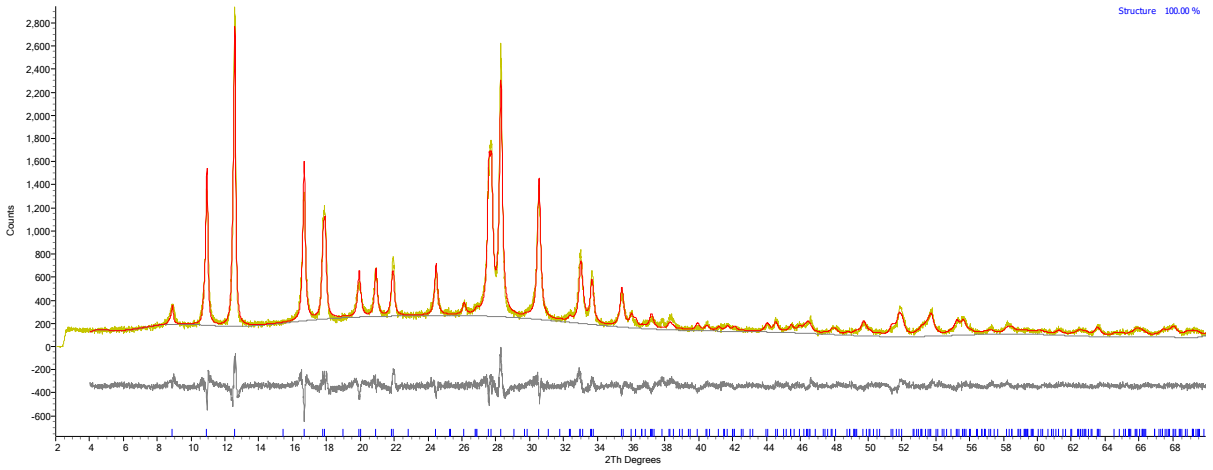


Figure S2.3. Rietveld fit of hydrated K-MER

Table S2.3. Refined structure of hydrated K-MER

| Site | Type | x | y | z | Occ | Mult | Biso |
|---|---|---|---|---|---|---|---|
| **K1** | K | 0 | 1 | 0.775(4) | 0.40(3) | 4 | 2 |
| **K2** | K | 0.5 | 0.8250(7) | 1 | 0.551(6) | 8 | 2 |
| **K3** | K | 0 | 0.5 | 0.806(11) | 0.133(11) | 4 | 2 |
| **Ow1** | O | 0 | 1 | 0.675(4) | 1.00(6) | 4 | 2 |
| **Ow2** | O | 0.5 | 0 | 0 | 0.43(3) | 4 | 2 |
| **Ow3** | O | 0.5 | 0.5 | 0.5 | 1.00(3) | 2 | 2 |
| **Ow4** | O | 0.4245(10) | 0.3404(7) | 0 | 0.665(7) | 16 | 2 |
| **O1** | O | 0.1447(13) | 0.1631(12) | 0.1920(13) | 1 | 16 | 1 |
| **O2** | O | 0.1190(8) | 0.2855(7) | 0 | 1 | 16 | 1 |
| **O3** | O | 0 | 0.2704(15) | 0.2176(19) | 1 | 8 | 1 |
| **O5** | O | 0.7885(15) | 0 | 0.189(2) | 1 | 8 | 1 |
| **O4** | O | 0.1745(13) | 0.3502(13) | 0.2412(17) | 1 | 16 | 1 |
| **Si1** | Si | 0.1102(6) | 0.2677(5) | 0.1633(11) | 0.8 | 16 | 1 |
| **Al1** | Al | 0.1102(6) | 0.2677(5) | 0.1633(11) | 0.2 | 16 | 1 |
| **Si2** | Si | 0.7531(5) | 0.1105(7) | 0.1559(11) | 0.8 | 16 | 1 |
| **Al2** | Al | 0.7531(5) | 0.1105(7) | 0.1559(11) | 0.2 | 16 | 1 |

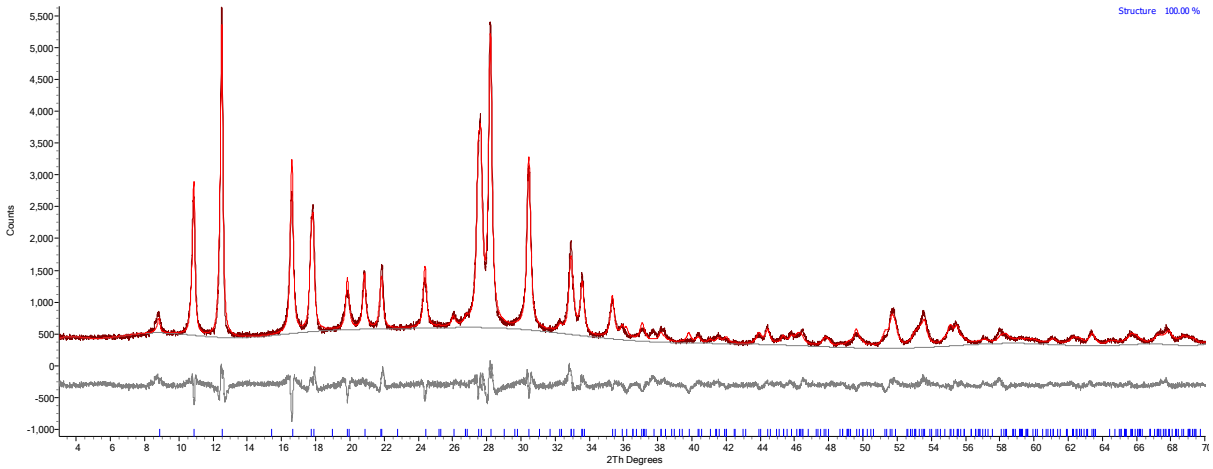


Figure S2.4. Rietveld fit of hydrated K,H-MER

Table S2.4. Refined structure of hydrated K,H-MER

| Site | Type | x | y | z | Occ | Mult | Biso |
|---|---|---|---|---|---|---|---|
| **K1** | K | 0 | 1 | 0.774(3) | 0.437(17) | 4 | 2 |
| **K2** | K | 0.5 | 0.8238(6) | 1 | 0.565(5) | 8 | 2 |
| **K3** | K | 0 | 0.5 | 0.801(8) | 0.164(10) | 4 | 2 |
| **Ow1** | O | 0 | 1 | 0.665(3) | 1.00(4) | 4 | 2 |
| **Ow2** | O | 0.5 | 0 | 0 | 0.54(2) | 4 | 2 |
| **Ow3** | O | 0.5 | 0.5 | 0.5 | 1.00(3) | 2 | 2 |
| **Ow4** | O | 0.4239(8) | 0.3377(6) | 0 | 0.694(6) | 16 | 2 |
| **O1** | O | 0.1451(14) | 0.1603(13) | 0.1890(11) | 1 | 16 | 1 |
| **O2** | O | 0.1173(7) | 0.2871(6) | 0 | 1 | 16 | 1 |
| **O3** | O | 0 | 0.2692(14) | 0.2165(19) | 1 | 8 | 1 |
| **O5** | O | 0.7809(14) | 0 | 0.192(2) | 1 | 8 | 1 |
| **O4** | O | 0.1716(13) | 0.3487(13) | 0.2417(18) | 1 | 16 | 1 |
| **Si1** | Si | 0.1116(7) | 0.2644(6) | 0.1628(12) | 0.8 | 16 | 1 |
| **Al1** | Al | 0.1116(7) | 0.2644(6) | 0.1628(12) | 0.2 | 16 | 1 |
| **Si2** | Si | 0.7503(5) | 0.1114(8) | 0.1597(12) | 0.8 | 16 | 1 |
| **Al2** | Al | 0.7503(5) | 0.1114(8) | 0.1597(12) | 0.2 | 16 | 1 |

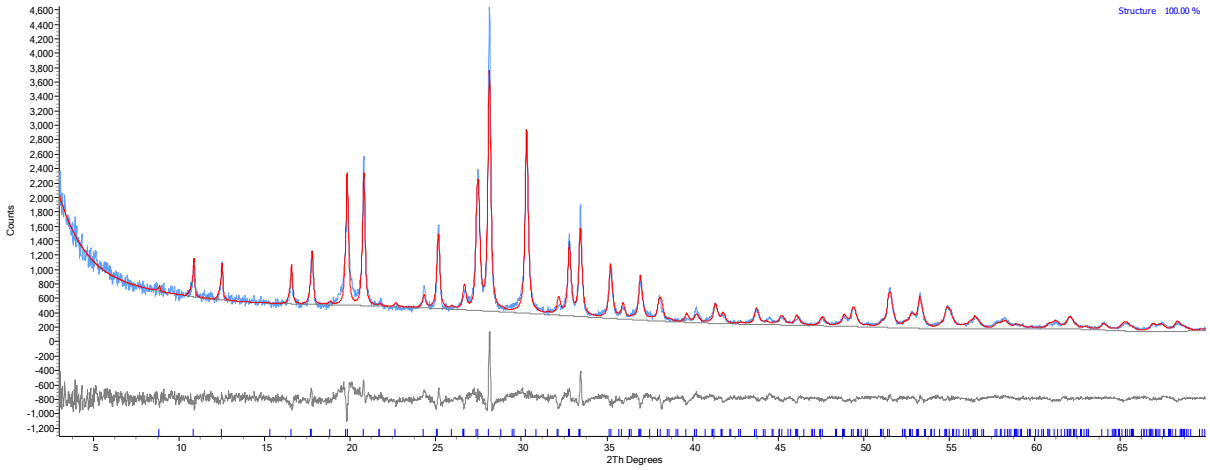


Figure S2.5. Rietveld fit of hydrated Cs-MER (flat plate geometry)

Table S2.5. Refined structure of hydrated Cs-MER

| Site | Type | x | y | z | Occ | Mult | Biso |
|---|---|---|---|---|---|---|---|
| **O2** | O | 0.1296(11) | 0.2885(11) | 0 | 1 | 16 | 1 |
| **O3** | O | 0 | 0.252(5) | 0.186(9) | 1 | 8 | 1 |
| **O5** | O | 0.751(6) | 0 | 0.183(9) | 1 | 8 | 1 |
| **O1** | O | 0.163(5) | 0.164(5) | 0.1891(16) | 1 | 16 | 1 |
| **O4** | O | 0.16(2) | 0.35(2) | 0.250(6) | 1 | 16 | 1 |
| **Si1** | Si | 0.112(2) | 0.261(3) | 0.160(2) | 0.8 | 16 | 1 |
| **Al1** | Al | 0.112(2) | 0.261(3) | 0.160(2) | 0.2 | 16 | 1 |
| **Si2** | Si | 0.741(3) | 0.111(2) | 0.161(2) | 0.8 | 16 | 1 |
| **Al2** | Al | 0.741(3) | 0.111(2) | 0.161(2) | 0.2 | 16 | 1 |
| **Cs1** | Cs | 0 | 1 | 0.7330(6) | 0.590(6) | 4 | 2 |
| **Cs2** | Cs | 0.5 | 0.8118(4) | 1 | 0.464(3) | 8 | 2 |
| **Cs3** | Cs | 0 | 0.5 | 0.801(2) | 0.249(5) | 4 | 2 |
| **Ow1** | O | 0.5 | 0 | 0 | 0.79(5) | 4 | 2 |
| **Ow2** | O | 0.5 | 0.5 | 0.5 | 1.00(6) | 2 | 2 |
| **Ow3** | O | 0.5 | 0.5 | 0 | 0.85(6) | 2 | 2 |
| **Ow4** | O | 0.3748(14) | 0.3748(14) | 0 | 0.74(2) | 8 | 2 |

## S3. Structural response to dehydration

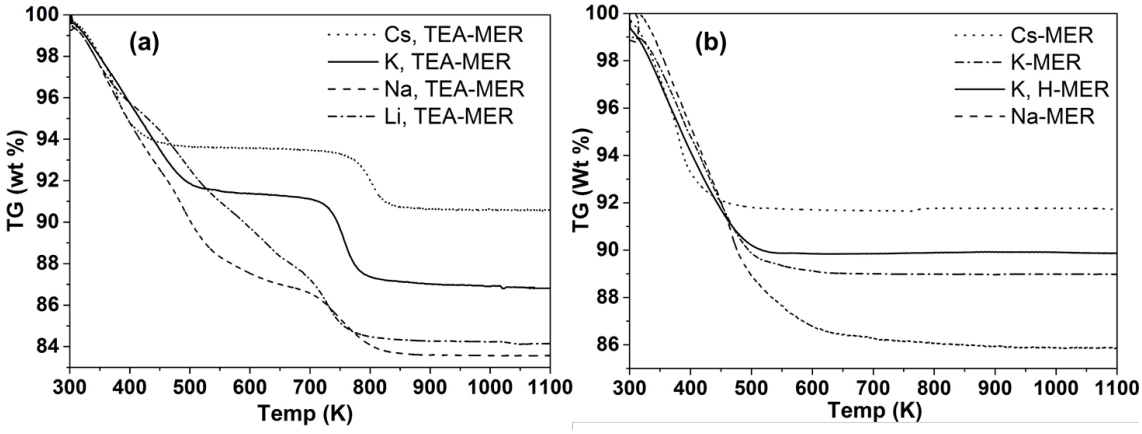


Figure S3.1. TGA curves of (a) M,TEA-MER and (b) M-MER zeolite samples.

## Crystallographic details of the refined dehydrated M,TEA-MER and M-MER

Table S3.1. Crystallographic details of the refinements of dehydrated M,TEA-MER

| **Sample** | **Li,TEA-MER** | **Na,TEA-MER** | **K,TEA-MER** | **Cs,TEA-MER** |
|---|---|---|---|---|
| **Unit Cell** | $N_{0.5}Si_{32}O_{64}$ | $Na_{5.8}N_{0.5}Si_{32}O_{64}$ | $K_{6.5}N_{0.5}Si_{32}O_{64}$ | $Cs_{6.6}N_{0.5}Si_{32}O_{64}$ |
| **T (K)** | 298 | 298 | 298 | 298 |
| **Space Group** | *Immm* | *Immm* | $P4_2/nmc$ | $P4_2/nmc$ |
| **X-ray Source** | Stoe | Stoe | Stoe | Stoe |
| **λ (Å)** | 1.54056 | 1.54056 | 1.54056 | 1.54056 |
| **a (Å)** | 13.198(1) | 13.522(1) | 13.650(1) | 13.791(1) |
| **b (Å)** | 13.257(2) | 13.547(1) | - | - |
| **c (Å)** | 10.140(1) | 10.098(1) | 9.997(1) | 10.042(1) |
| **V (Å$^3$)** | 1774(1) | 1850(1) | 1863(1) | 1910(1) |
| $R_p$ | 7.5% | 6.0% | 6.7% | 5.5% |
| $R_{wp}$ | 9.4% | 7.8% | 8.7% | 7.4% |
| $\chi^2$ | 2.6 | 2.3 | 2.3 | 1.3 |

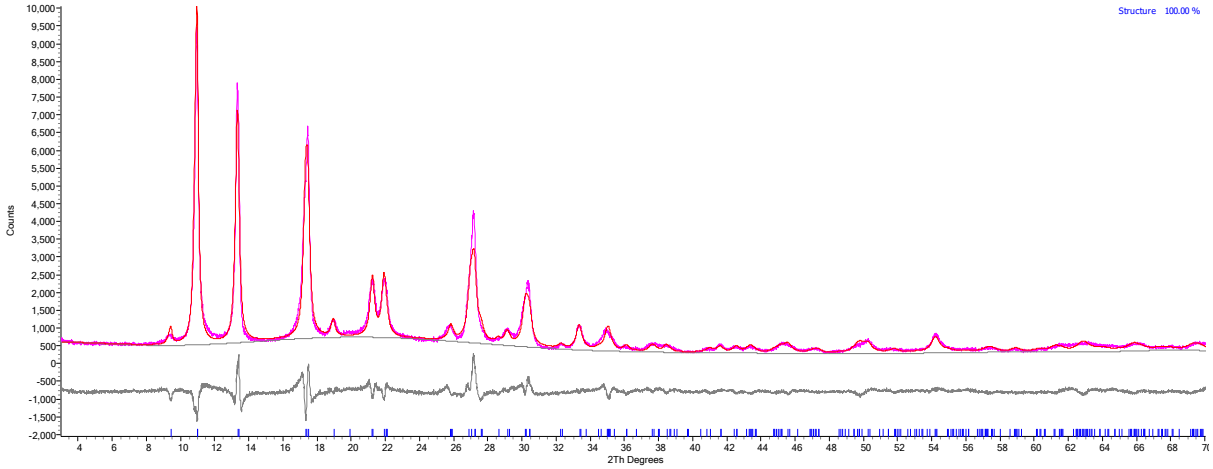


Figure S3.2. Rietveld fit of dehydrated Li,TEA-MER

Table S3.2. Refined structure of dehydrated Li,TEA-MER

| Site | Type | x | y | z | Occ | Mult | Biso |
|---|---|---|---|---|---|---|---|
| **O1** | O | 0.1957(12) | 0.1244(12) | 0.1973(14) | 1 | 16 | 1 |
| **O2** | O | 0.1223(14) | 0.2631(13) | 0 | 1 | 8 | 1 |
| **O5** | O | 0.6489(18) | 0.1519(14) | 0 | 1 | 8 | 1 |
| **O3** | O | 0 | 0.1586(15) | 0.180(3) | 1 | 8 | 1 |
| **O6** | O | 0.6555(16) | 0 | 0.190(3) | 1 | 8 | 1 |
| **O4** | O | 0.1260(12) | 0.2973(14) | 0.2488(19) | 1 | 16 | 1 |
| **Si1** | Si | 0.1074(7) | 0.2067(8) | 0.1591(11) | 0.8 | 16 | 1 |
| **Al1** | Al | 0.1074(7) | 0.2067(8) | 0.1591(11) | 0.2 | 16 | 1 |
| **Si2** | Si | 0.6805(7) | 0.1133(7) | 0.1610(12) | 0.8 | 16 | 1 |
| **Al2** | Al | 0.6805(7) | 0.1133(7) | 0.1610(12) | 0.2 | 16 | 1 |
| **N** | N | 0.5 | 0.5 | 0 | 0.25 | 2 | 2 |

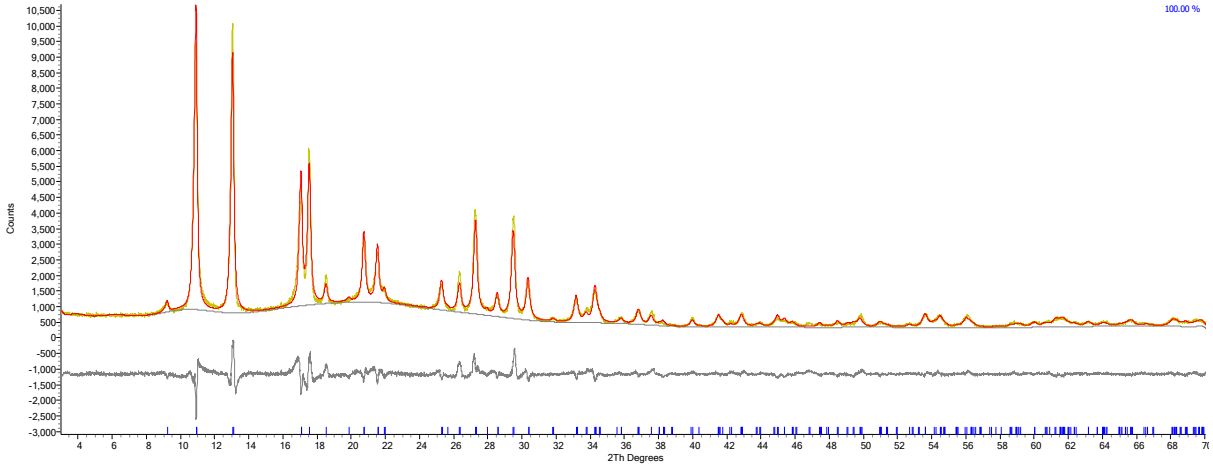


Figure S3.3. Rietveld fit of dehydrated Na,TEA-MER

Table S3.3. Refined structure of dehydrated Na,TEA-MER

| Site | Type | x | y | z | Occ | Mult | Biso |
|---|---|---|---|---|---|---|---|
| **Na1** | Na | 0.046(2) | 1 | 0.7713(16) | 0.426(15) | 8 | 2 |
| **Na2** | Na | 0.5 | 0.769(3) | 1(2) | 0.245(13) | 8 | 2 |
| **Na3** | Na | 0 | 0.5 | 0.968(10) | 0.268(15) | 4 | 2 |
| **N1** | N | 0.5 | 0.5 | 0 | 0.25 | 2 | 2 |
| **O1** | O | 0.1841(12) | 0.1352(11) | 0.1839(15) | 1 | 16 | 1 |
| **O2** | O | 0.1200(17) | 0.2723(14) | 0 | 1 | 8 | 1 |
| **O5** | O | 0.6692(15) | 0.1346(13) | 0 | 1 | 8 | 1 |
| **O3** | O | 0 | 0.1827(13) | 0.181(2) | 1 | 8 | 1 |
| **O6** | O | 0.6764(15) | 0 | 0.213(2) | 1 | 8 | 1 |
| **O4** | O | 0.1293(12) | 0.3070(13) | 0.2612(15) | 1 | 16 | 1 |
| **Si1** | Si | 0.1120(6) | 0.2272(7) | 0.1536(11) | 0.8 | 16 | 1 |
| **Al1** | Al | 0.1120(6) | 0.2272(7) | 0.1536(11) | 0.2 | 16 | 1 |
| **Si2** | Si | 0.6952(6) | 0.1130(6) | 0.1648(8) | 0.8 | 16 | 1 |
| **Al2** | Al | 0.6952(6) | 0.1130(6) | 0.1648(8) | 0.2 | 16 | 1 |

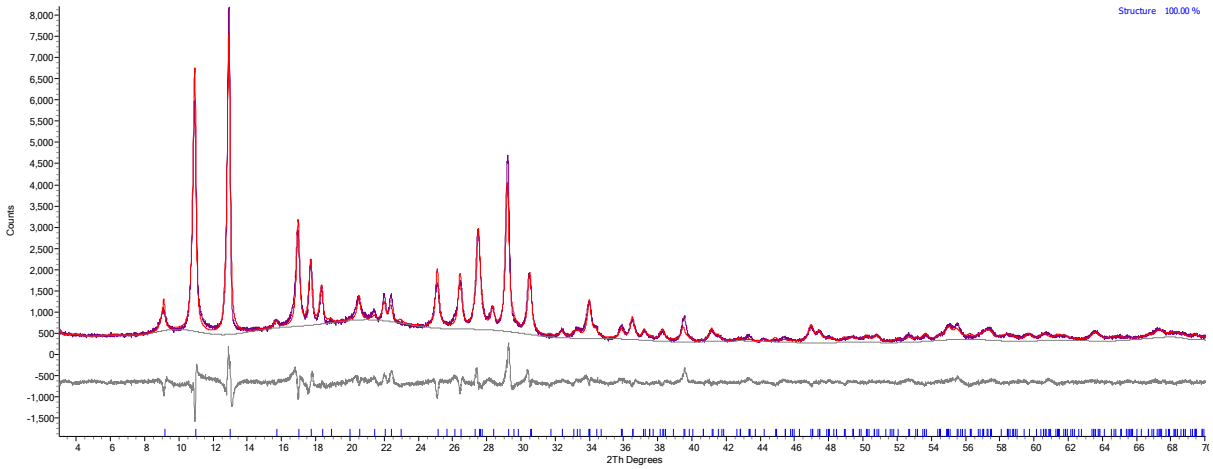


Figure S3.4. Rietveld fit of dehydrated K,TEA-MER

Table S3.4. Refined structure of dehydrated K,TEA-MER

| Site | Type | x | y | z | Occ | Mult | Biso |
|---|---|---|---|---|---|---|---|
| **O1** | O | 0.1302(10) | 0.6955(10) | 0.5405(16) | 1 | 16 | 1 |
| **O2** | O | 0.1376(9) | -0.1794(11) | 0.3123(15) | 1 | 16 | 1 |
| **O3** | O | -0.6926(11) | -0.1331(10) | 0.1893(16) | 1 | 16 | 1 |
| **O4** | O | 0 | 0.6977(13) | 0.315(2) | 1 | 8 | 1 |
| **O5** | O | 0.1971(14) | 0 | 0.331(2) | 1 | 8 | 1 |
| **Si1** | Si | 0.1127(5) | 0.7148(6) | 0.3629(9) | 0.8 | 16 | 1 |
| **Al1** | Al | 0.1127(5) | 0.7148(6) | 0.3629(9) | 0.2 | 16 | 1 |
| **Si2** | Si | 0.2465(5) | -0.1094(5) | 0.3302(9) | 0.8 | 16 | 1 |
| **Al2** | Al | 0.2465(5) | -0.1094(5) | 0.3302(9) | 0.2 | 16 | 1 |
| **K1** | K | 0.5 | 0.5 | -0.099(2) | 0.356(6) | 4 | 2 |
| **K2** | K | 0.2706(12) | 0.5 | 0.529(2) | 0.385(6) | 8 | 2 |
| **K3** | K | 0 | 0.5 | 0.138(3) | 0.476(9) | 4 | 2 |
| **N1** | N | 0.5 | 0.5 | 0.5 | 0.25 | 2 | 2 |

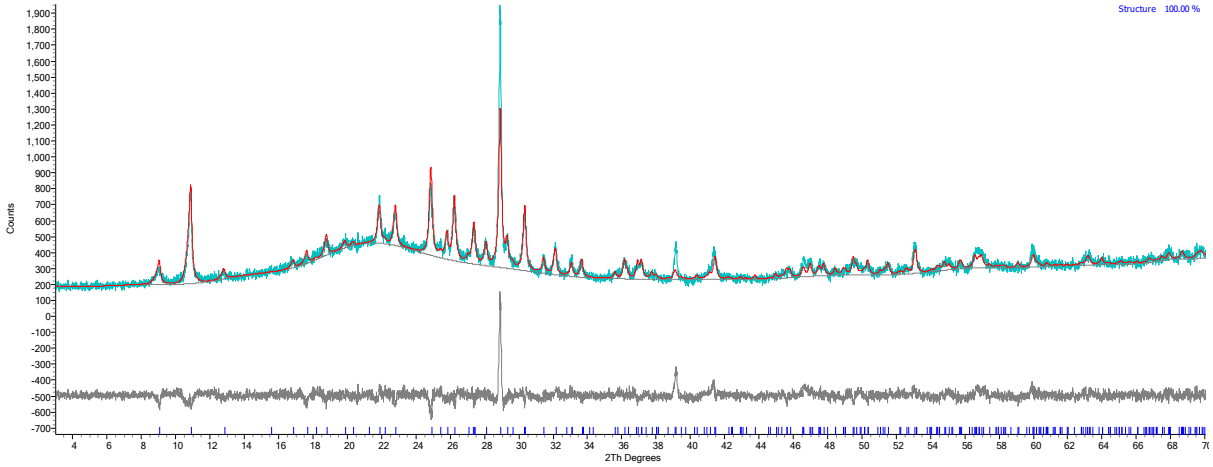


Figure S3.5. Rietveld fit of dehydrated Cs,TEA-MER

Table S3.5. Refined structure of dehydrated Cs,TEA-MER

| Site | Type | x | y | z | Occ | Mult | Biso |
|---|---|---|---|---|---|---|---|
| **O1** | O | 0.118(2) | 0.7155(18) | 0.523(3) | 1 | 16 | 1 |
| **O2** | O | 0.143(2) | -0.174(3) | 0.305(3) | 1 | 16 | 1 |
| **O3** | O | -0.685(3) | -0.136(3) | 0.205(3) | 1 | 16 | 1 |
| **O4** | O | 0 | 0.708(3) | 0.302(4) | 1 | 8 | 1 |
| **O5** | O | 0.208(3) | 0 | 0.300(4) | 1 | 8 | 1 |
| **Si1** | Si | 0.1102(11) | 0.7300(13) | 0.3497(18) | 0.8 | 16 | 1 |
| **Al1** | Al | 0.1102(11) | 0.7300(13) | 0.3497(18) | 0.2 | 16 | 1 |
| **Si2** | Si | 0.2446(13) | -0.1086(12) | 0.3279(17) | 0.8 | 16 | 1 |
| **Al2** | Al | 0.2446(13) | -0.1086(12) | 0.3279(17) | 0.2 | 16 | 1 |
| **Cs1** | Cs | 0.5 | 0.5 | 0 | 0.682(11) | 2 | 2 |
| **Cs2** | Cs | 0.2888(13) | 0.5 | 0.532(2) | 0.274(5) | 8 | 2 |
| **Cs3** | Cs | 0 | 0.5 | 0.1190(10) | 0.756(8) | 4 | 2 |
| **N1** | N | 0.5 | 0.5 | 0.5 | 0.25 | 2 | 2 |

Table S3.6. Crystallographic details of the refinements of dehydrated M-MER

| **Sample** | **Na-MER** | **K,H-MER** | **K-MER** | **Cs-MER** |
|---|---|---|---|---|
| **Unit Cell** | $Na_{6.8}Si_{32}O_{64}$ | $K_{6.6}Si_{32}O_{64}$ | $K_{6.5}Si_{32}O_{64}$ | $Cs_{6.0}Si_{32}O_{64}$ |
| **T (K)** | 298 | 298 | 298 | 298 |
| **Space Group** | *Immm* | $P4_2/nmc$ | $P4_2/nmc$ | $P4_2/nmc$ |
| **X-ray Source** | Stoe | Stoe | Stoe | Stoe |
| **λ (Å)** | 1.54056 | 1.54056 | 1.54056 | 1.54056 |
| **a (Å)** | 13.493(1) | 13.544(1) | 13.586(1) | 13.751(1) |
| **b (Å)** | 13.520(1) | - | - | - |
| **c (Å)** | 9.914(1) | 9.856(1) | 9.876(1) | 9.950(1) |
| **V (Å$^3$)** | 1809(1) | 1808(1) | 1823(1) | 1881(1) |
| $\boldsymbol{R_p}$ | 6.1% | 6.1% | 6.4% | 7.9% |
| $\boldsymbol{R_{wp}}$ | 8.2% | 8.0% | 8.1% | 9.3% |
| $\boldsymbol{\chi^2}$ | 2.5 | 2.1 | 1.7 | 1.2 |

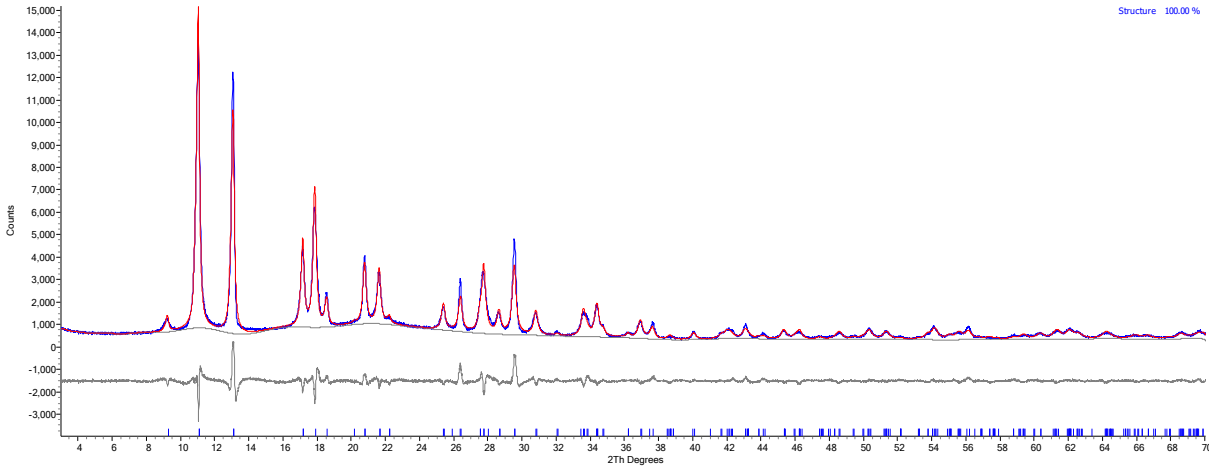


Figure S3.6. Rietveld fit of dehydrated Na-MER

Table S3.7. Refined structure of dehydrated Na-MER

| Site | Type | x | y | z | Occ | Mult | Biso |
|---|---|---|---|---|---|---|---|
| **Na1** | Na | 0.054(2) | 1 | 0.796(2) | 0.396(17) | 8 | 2 |
| **Na2** | Na | 0.5 | 0.784(2) | 0.973(8) | 0.329(13) | 8 | 2 |
| **Na3** | Na | 0 | 0.5 | 0.843(9) | 0.221(18) | 4 | 2 |
| **O1** | O | 0.1886(11) | 0.1269(10) | 0.1838(14) | 1 | 16 | 1 |
| **O2** | O | 0.1141(15) | 0.2604(13) | 0 | 1 | 8 | 1 |
| **O5** | O | 0.6609(13) | 0.1261(13) | 0 | 1 | 8 | 1 |
| **O3** | O | 0 | 0.1774(15) | 0.201(2) | 1 | 8 | 1 |
| **O6** | O | 0.6631(15) | 0 | 0.229(2) | 1 | 8 | 1 |
| **O4** | O | 0.1274(10) | 0.2962(14) | 0.2730(16) | 1 | 16 | 1 |
| **Si1** | Si | 0.1114(6) | 0.2238(7) | 0.1540(10) | 0.8 | 16 | 1 |
| **Al1** | Al | 0.1114(6) | 0.2238(7) | 0.1540(10) | 0.2 | 16 | 1 |
| **Si2** | Si | 0.6901(6) | 0.1102(7) | 0.1653(8) | 0.8 | 16 | 1 |
| **Al2** | Al | 0.6901(6) | 0.1102(7) | 0.1653(8) | 0.2 | 16 | 1 |

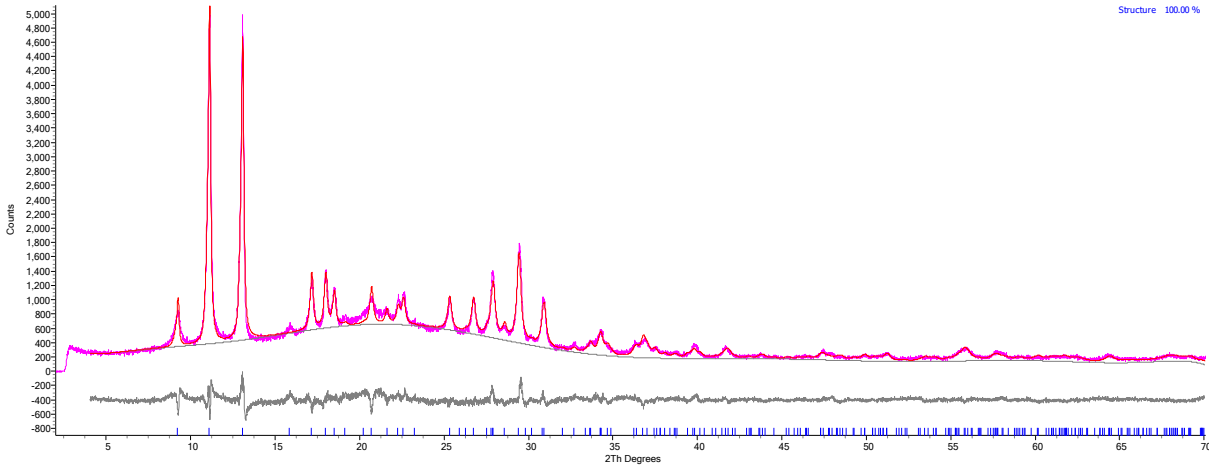


Figure S3.7. Rietveld fit of dehydrated K-MER

Table 3.8. Refined structure of dehydrated K-MER

| Site | Type | x | y | z | Occ | Mult | Biso |
|---|---|---|---|---|---|---|---|
| **O1** | O | 0.1310(10) | 0.6908(10) | 0.5246(17) | 1 | 16 | 1 |
| **O2** | O | 0.1453(10) | -0.1796(11) | 0.3323(15) | 1 | 16 | 1 |
| **O3** | O | -0.6929(11) | -0.1246(12) | 0.2071(15) | 1 | 16 | 1 |
| **O4** | O | 0 | 0.6899(13) | 0.309(2) | 1 | 8 | 1 |
| **O5** | O | 0.1872(12) | 0 | 0.380(2) | 1 | 8 | 1 |
| **Si1** | Si | 0.1097(6) | 0.7102(5) | 0.3503(9) | 0.8 | 16 | 1 |
| **A11** | Al | 0.1097(6) | 0.7102(5) | 0.3503(9) | 0.2 | 16 | 1 |
| **Si2** | Si | 0.2419(5) | -0.1169(6) | 0.3284(10) | 0.8 | 16 | 1 |
| **Al2** | Al | 0.2419(5) | -0.1169(6) | 0.3284(10) | 0.2 | 16 | 1 |
| **K1** | K | 0.5 | 0.5 | -0.088(2) | 0.376(6) | 4 | 2 |
| **K2** | K | 0.2219(11) | 0.5 | 0.5720(16) | 0.477(7) | 8 | 2 |
| **K3** | K | 0 | 0.5 | 0.177(5) | 0.281(8) | 4 | 2 |

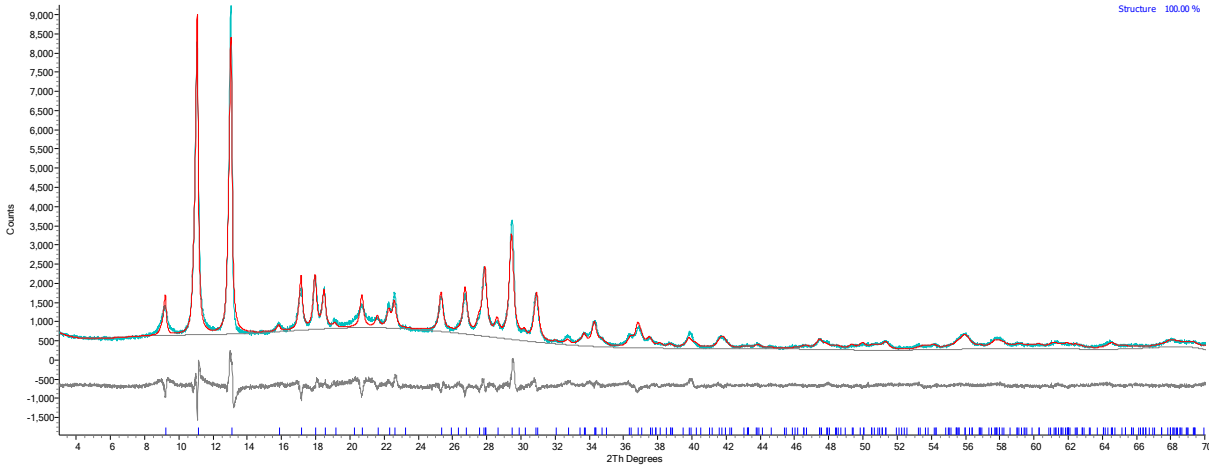


Figure S3.8. Rietveld fit of dehydrated K,H-MER

Table 3.9. Refined structure of dehydrated K,H-MER

| Site | Type | x | y | z | Occ | Mult | Biso |
|---|---|---|---|---|---|---|---|
| **O1** | O | 0.1300(10) | 0.6952(10) | 0.5391(17) | 1 | 16 | 1 |
| **O2** | O | 0.1415(9) | -0.1793(9) | 0.3206(12) | 1 | 16 | 1 |
| **O3** | O | -0.6962(9) | -0.1217(9) | 0.1915(13) | 1 | 16 | 1 |
| **O4** | O | 0 | 0.6924(11) | 0.312(2) | 1 | 8 | 1 |
| **O5** | O | 0.1864(11) | 0 | 0.3433(19) | 1 | 8 | 1 |
| **Si1** | Si | 0.1125(5) | 0.7095(5) | 0.3643(8) | 0.8 | 16 | 1 |
| **Al1** | Al | 0.1125(5) | 0.7095(5) | 0.3643(8) | 0.2 | 16 | 1 |
| **Si2** | Si | 0.2399(5) | -0.1135(5) | 0.3244(9) | 0.8 | 16 | 1 |
| **Al2** | Al | 0.2399(5) | -0.1135(5) | 0.3244(9) | 0.2 | 16 | 1 |
| **K1** | K | 0.5 | 0.5 | -0.0808(18) | 0.398(5) | 4 | 2 |
| **K2** | K | 0.2227(9) | 0.5 | 0.5558(15) | 0.445(6) | 8 | 2 |
| **K3** | K | 0 | 0.5 | 0.143(3) | 0.331(7) | 4 | 2 |

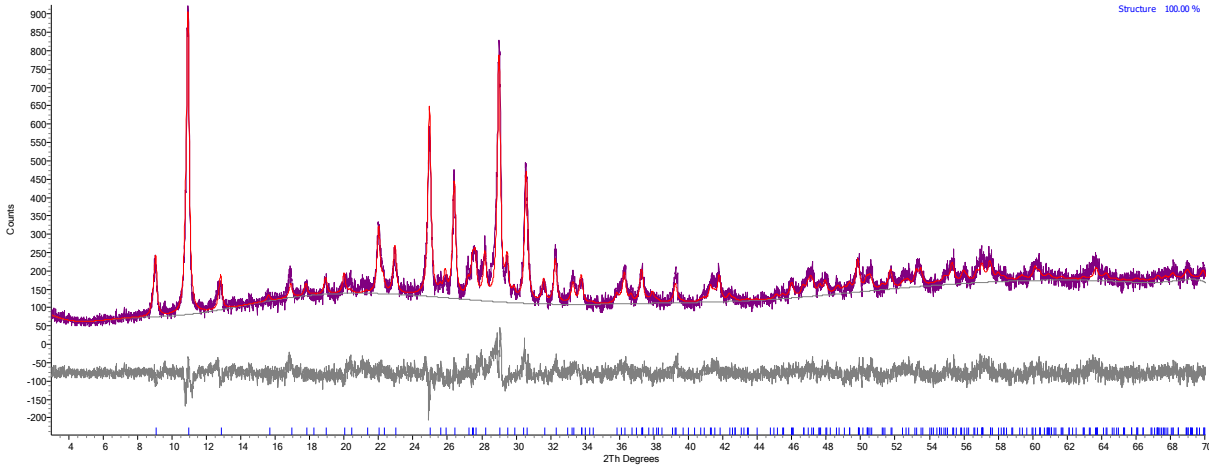


Figure S3.9. Rietveld fit of dehydrated Cs-MER

Table S3.10. Refined structure of dehydrated Cs-MER

| Site | Type | x | y | z | Occ | Mult | Biso |
|---|---|---|---|---|---|---|---|
| **O1** | O | 0.1218(16) | 0.7013(15) | 0.527(3) | 1 | 16 | 1 |
| **O2** | O | 0.1486(18) | -0.180(2) | 0.320(2) | 1 | 16 | 1 |
| **O3** | O | -0.682(2) | -0.1340(18) | 0.208(3) | 1 | 16 | 1 |
| **O4** | O | 0 | 0.698(2) | 0.319(4) | 1 | 8 | 1 |
| **O5** | O | 0.206(2) | 0 | 0.314(3) | 1 | 8 | 1 |
| **Si1** | Si | 0.1132(9) | 0.7127(11) | 0.3613(18) | 0.8 | 16 | 1 |
| **Al1** | Al | 0.1132(9) | 0.7127(11) | 0.3613(18) | 0.2 | 16 | 1 |
| **Si2** | Si | 0.2445(12) | -0.1099(9) | 0.3308(18) | 0.8 | 16 | 1 |
| **Al2** | Al | 0.2445(12) | -0.1099(9) | 0.3308(18) | 0.2 | 16 | 1 |
| **Cs1** | Cs | 0.5 | 0.5 | 0 | 0.777(9) | 2 | 2 |
| **Cs2** | Cs | 0.2876(11) | 0.5 | 0.5248(17) | 0.240(4) | 8 | 2 |
| **Cs3** | Cs | 0 | 0.5 | 0.1204(10) | 0.621(6) | 4 | 2 |

## S4. Adsorption studies

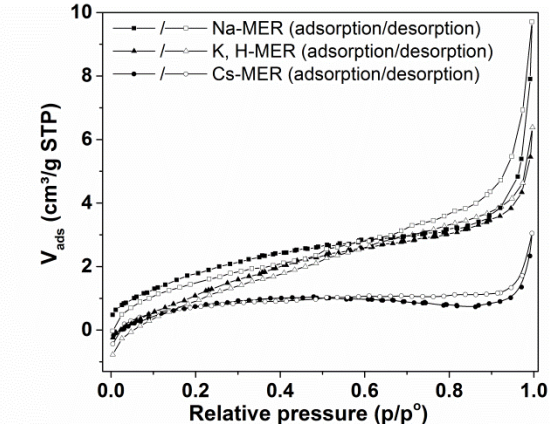


Figure S4.1. $N_2$ adsorption/desorption isotherms at 77 K of Na-, K, H- and Cs-MER

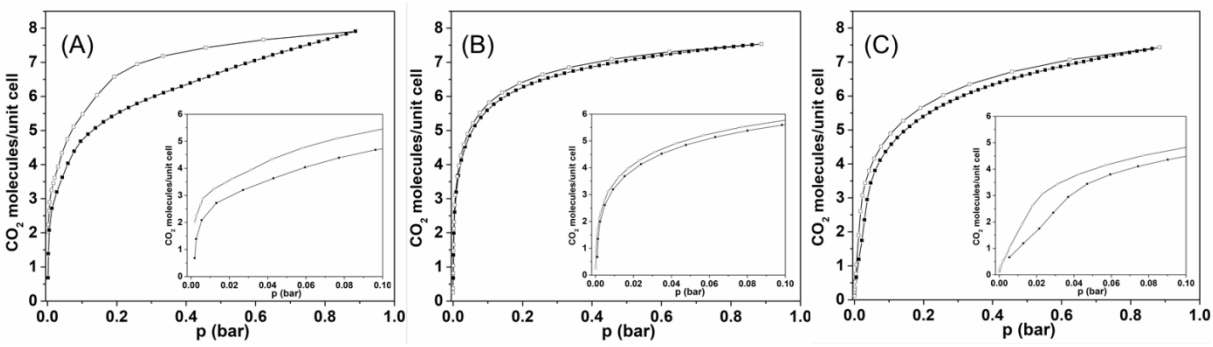


Figure S4.2. $CO_2$ adsorption isotherms (0 - 1 bar at 298 K) of (A) Na-, (B) K- and (C) Cs-MER, with molecules of $CO_2$ per unit cell on the y axis.

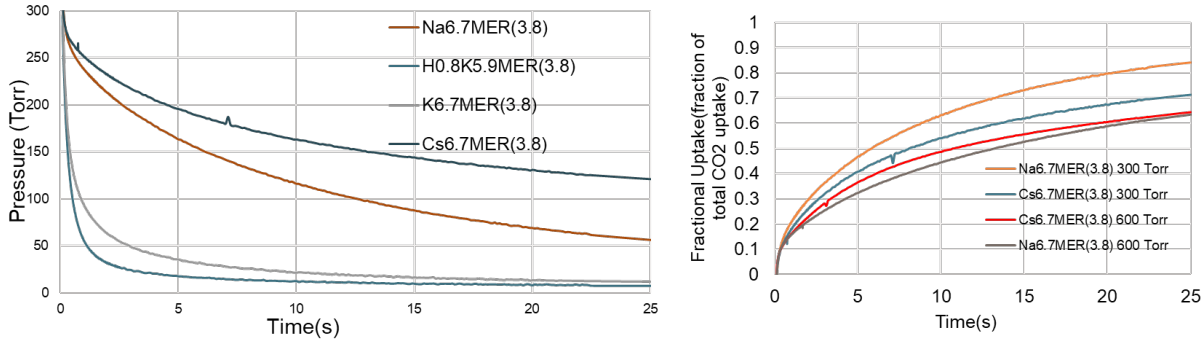


Figure S4.3. Absolute uptake curves for Na-MER, K,H-MER, K-MER, and Cs-MER; and fractional uptake curves for Na-MER and Cs-MER at 0.4 and 0.8 bar

**S5. In situ laboratory PXRD of M-MER with adsorbed $CO_2$**

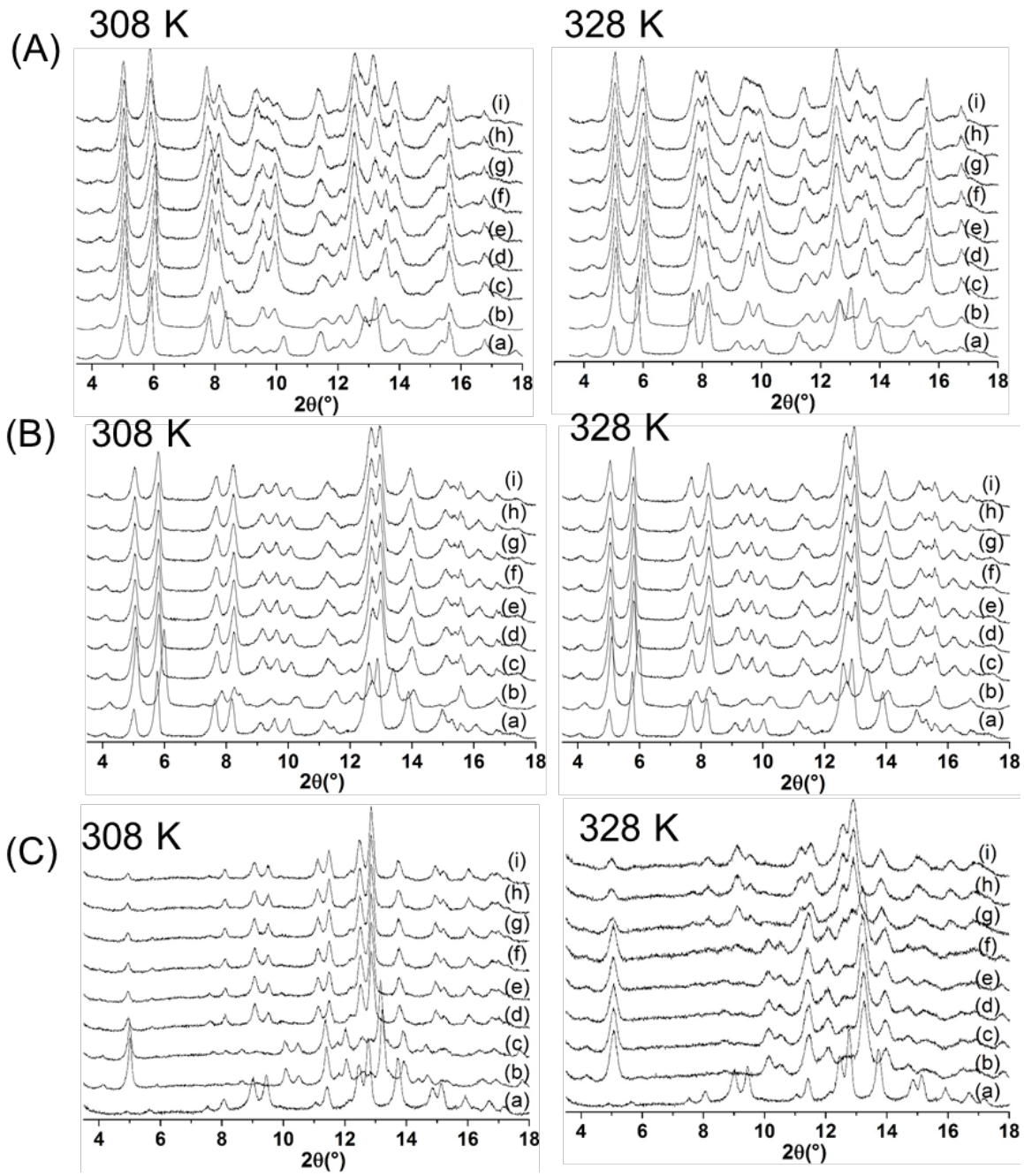


Figure S5.1. PXRD of (A) Na-MER, (B) K-MER and (C) Cs-MER, where (a) hydrated, (b) dehydrated and measured with $CO_2$ adsorbed at different temperatures at different pressures (in bar): (c) 0.1, (d) 0.2, (e) 0.3, (f) 0.4, (g) 0.6, (h) 0.8, (i) 1.

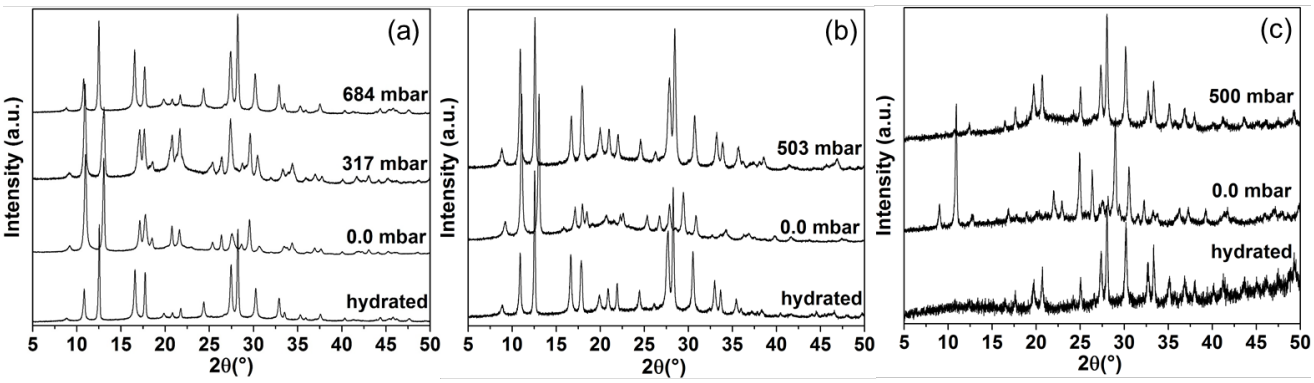


Figure S5.2. Capillary PXRD of (a) Na-MER, (b) K-MER and (c) Cs-MER loaded with $CO_2$ at different pressures

## S6. Structure of $CO_2$-loaded merlinoite samples

Table S6.1. Crystallographic details of the refined dehydrated solids with adsorbed $CO_2$

| **Sample** | **Na-MER (317 mbar)** | **Na-MER (684 mbar)** | **K-MER (500 mbar)** | **K,H-MER (536 mbar)** | **Cs-MER (500 mbar)** |
|---|---|---|---|---|---|
| **Unit Cell** | $Na_{6.7}Si_{32}O_{64}.(CO_2)_{4.9}$ | $Na_{6.8}Si_{32}O_{64}.(CO_2)_{7.6}$ | $K_{7.0}Si_{32}O_{64}.(CO_2)_{5.8}$ | $K_{7.0}Si_{32}O_{64}.(CO_2)_{4.4}$ | $Cs_{6.7}Si_{32}O_{64}.(CO_2)_{7.4}$ |
| **T (K)** | 298 | 298 | 298 | 298 | 298 |
| **Space Group** | *Immm* | *Immm* | $P4_2/nmc$ | $P4_2/nmc$ | $P4_2/nmc$ |
| **X-ray Source** | Stoe | Stoe | Stoe | Stoe | Stoe |
| **λ (Å)** | 1.54056 | 1.54056 | 1.54056 | 1.54056 | 1.54056 |
| **a (Å)** | 13.477(1) | 14.121(1) | 13.990(1) | 13.989(1) | 14.197(1) |
| **b (Å)** | 13.441(1) | 14.122(1) | - | - | - |
| **c (Å)** | 10.015(1) | 10.031(1) | 9.832(1) | 9.835(1) | 10.016(1) |
| **V (Å$^3$)** | 1814(1) | 2000(1) | 1924(1) | 1925(1) | 2019(1) |
| $R_p$ | 5.9% | 5.3% | 6.5% | 5.1% | 6.0% |
| $R_{wp}$ | 7.8% | 7.0% | 8.3% | 6.6% | 7.5% |
| $\chi^2$ | 2.3 | 2.1 | 1.7 | 1.8 | 1.2 |

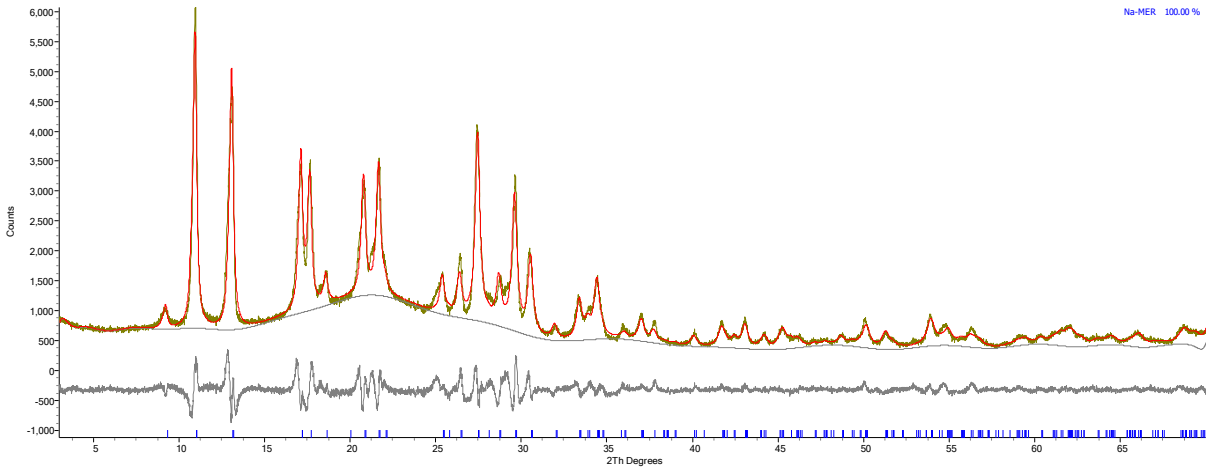


Figure S6.1. Rietveld profile for Na-MER (317 mbar $CO_2$)

Table S6.2. Refined structure of Na-MER (317 mbar $CO_2$)

| Site | Type | x | y | z | Occ | Mult | Biso |
|---|---|---|---|---|---|---|---|
| **Na1** | Na | 0.067(3) | 1 | 0.791(3) | 0.37(2) | 8 | 2 |
| **Na2** | Na | 0.5 | 0.802(6) | 0 | 0.39(3) | 4 | 2 |
| **Na3** | Na | 0 | 0.5 | 0.253(7) | 0.56(3) | 4 | 2 |
| **O1** | O | 0.1918(16) | 0.1253(15) | 0.179(3) | 1 | 16 | 1 |
| **O2** | O | 0.1335(17) | 0.2585(19) | 0 | 1 | 8 | 1 |
| **O5** | O | 0.665(2) | 0.1233(18) | 0 | 1 | 8 | 1 |
| **O3** | O | 0 | 0.167(2) | 0.193(4) | 1 | 8 | 1 |
| **O6** | O | 0.657(2) | 0 | 0.210(3) | 1 | 8 | 1 |
| **O4** | O | 0.1270(14) | 0.308(2) | 0.252(3) | 1 | 16 | 1 |
| **Si1** | Si | 0.1117(9) | 0.2117(8) | 0.1535(12) | 0.8 | 16 | 1 |
| **Al1** | Al | 0.1117(9) | 0.2117(8) | 0.1535(12) | 0.2 | 16 | 1 |
| **Si2** | Si | 0.6856(10) | 0.1139(8) | 0.1543(13) | 0.8 | 16 | 1 |
| **Al2** | Al | 0.6856(10) | 0.1139(8) | 0.1543(13) | 0.2 | 16 | 1 |
| **C1** | C | 0.5 | 0.5 | 0 | 0.44(2) | 2 | 2 |
| **OC1** | O | 0.5 | 0.5 | 0.115826 | 0.44(2) | 4 | 2 |
| **C2** | C | 0.2597(14) | 0 | 0.5 | 0.98(2) | 4 | 2 |
| **OC2** | O | 0.2597(14) | -0.0863 | 0.5 | 0.98(2) | 8 | 2 |

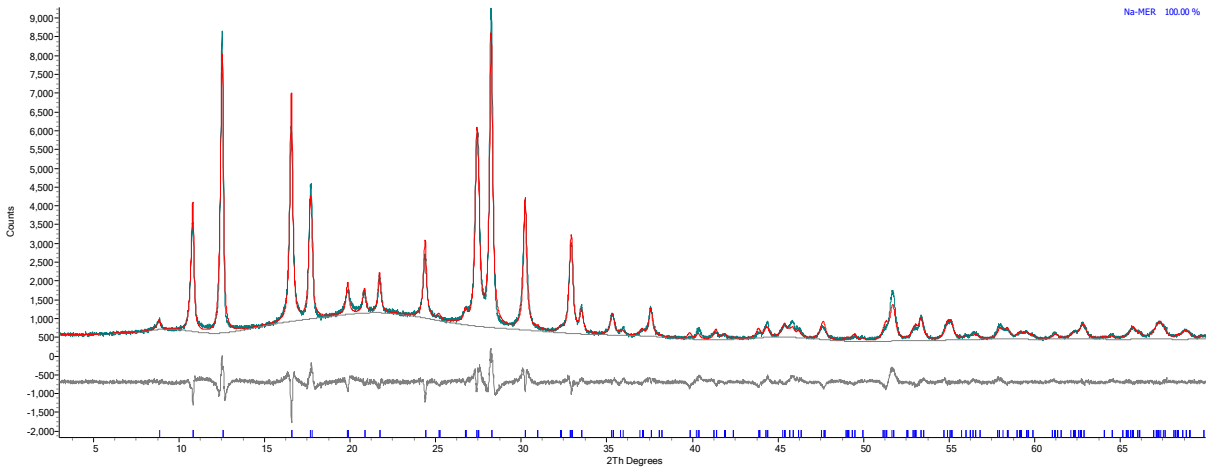


Figure S6.2. Rietveld refinement of Na-MER (684 mbar $CO_2$)

Table S6.3. Refined structure of Na-MER (684 mbar $CO_2$)

| Site | Type | x | y | z | Occ | Mult | Biso |
|---|---|---|---|---|---|---|---|
| **Na1** | Na | 0 | 1 | 0.227(6) | 0.27(3) | 4 | 2 |
| **Na2** | Na | 0.5 | 0.772(2) | 0 | 0.74(3) | 4 | 2 |
| **Na3** | Na | 0 | 0.5 | 0.687(4) | 0.68(3) | 4 | 2 |
| **O1** | O | 0.1654(19) | 0.1641(18) | 0.2005(11) | 1 | 16 | 1 |
| **O2** | O | 0.119(2) | 0.283(2) | 0 | 1 | 8 | 1 |
| **O5** | O | 0.706(2) | 0.1313(17) | 0 | 1 | 8 | 1 |
| **O3** | O | 0 | 0.247(2) | 0.203(2) | 1 | 8 | 1 |
| **O6** | O | 0.752(2) | 0 | 0.184(3) | 1 | 8 | 1 |
| **O4** | O | 0.1487(16) | 0.3530(16) | 0.247(3) | 1 | 16 | 1 |
| **Si1** | Si | 0.1035(8) | 0.2616(9) | 0.1598(12) | 0.8 | 16 | 1 |
| **Al1** | Al | 0.1035(8) | 0.2616(9) | 0.1598(12) | 0.2 | 16 | 1 |
| **Si2** | Si | 0.7380(10) | 0.1103(8) | 0.1555(14) | 0.8 | 16 | 1 |
| **Al2** | Al | 0.7380(10) | 0.1103(8) | 0.1555(14) | 0.2 | 16 | 1 |
| **C1** | C | 0.5 | 0.5 | 0 | 0.567(18) | 2 | 2 |
| **OC1** | O | 0.5 | 0.5 | 0.115645 | 0.567(18) | 4 | 2 |
| **C2** | C | 0.1800(10) | 0 | 0.5 | 1.000(19) | 4 | 2 |
| **OC2** | O | 0.1800(10) | -0.08214 | 0.5 | 1.000(19) | 8 | 2 |
| **C3** | C | 0 | 0.5 | 0 | 0.70(2) | 2 | 2 |
| **OC3** | O | 0.082148 | 0.5 | 0 | 0.70(2) | 4 | 2 |

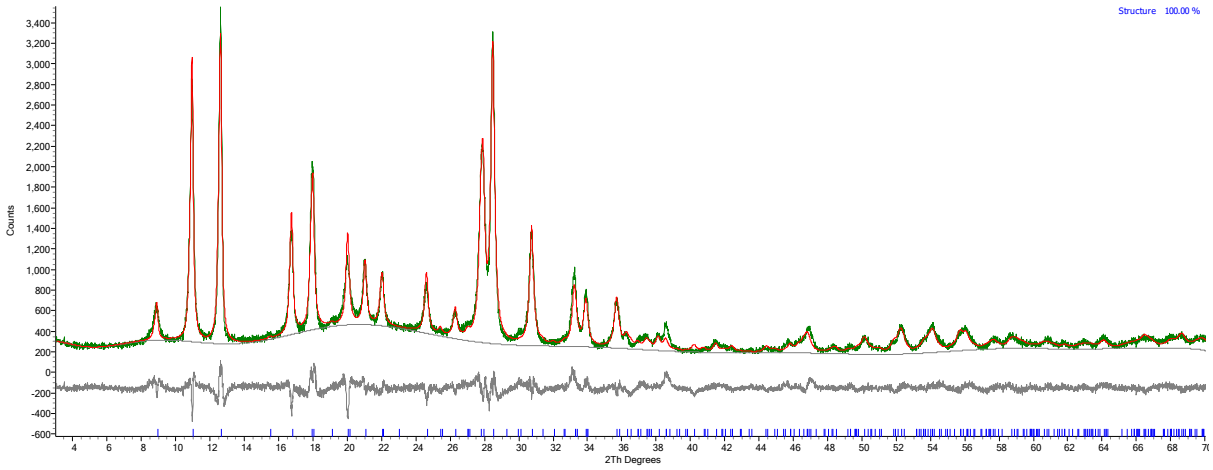


Figure S6.3. Rietveld plot of K-MER (500 mbar $CO_2$)

Table S6.4. Refined structure of K-MER (500 mbar $CO_2$)

| Site | Type | x | y | z | Occ | Mult | Biso |
|---|---|---|---|---|---|---|---|
| **K1** | K | 0 | 1 | 0.7689(19) | 0.406(17) | 4 | 2 |
| **K2** | K | 0.5 | 0.8126(7) | 1 | 0.545(6) | 8 | 2 |
| **K3** | K | 0 | 0.5 | 0.789(7) | 0.256(9) | 4 | 2 |
| **O1** | O | 0.1439(11) | 0.1661(11) | 0.1973(13) | 1 | 16 | 1 |
| **O2** | O | 0.1241(9) | 0.2824(9) | 0 | 1 | 16 | 1 |
| **O3** | O | 0 | 0.2856(18) | 0.209(2) | 1 | 8 | 1 |
| **O5** | O | 0.7874(15) | 0 | 0.187(2) | 1 | 8 | 1 |
| **O4** | O | 0.1765(11) | 0.3548(12) | 0.2363(14) | 1 | 16 | 1 |
| **Si1** | Si | 0.1144(6) | 0.2704(5) | 0.1638(10) | 0.8 | 16 | 1 |
| **Al1** | Al | 0.1144(6) | 0.2704(5) | 0.1638(10) | 0.2 | 16 | 1 |
| **Si2** | Si | 0.7583(5) | 0.1071(6) | 0.1616(11) | 0.8 | 16 | 1 |
| **Al2** | Al | 0.7583(5) | 0.1071(6) | 0.1616(11) | 0.2 | 16 | 1 |
| **C1** | C | 0.5 | 0.5 | 0 | 0.714(15) | 2 | 2 |
| **OC1** | O | 0.5 | 0.5 | 0.117979 | 0.714(15) | 4 | 2 |
| **C2** | C | 0.1835(14) | 0 | 0.5 | 0.297(7) | 8 | 2 |
| **OC2** | O | 0.1835(14) | -0.08292 | 0.5 | 0.297(7) | 16 | 2 |
| **C6** | C | 0 | 0 | 0 | 0.942(18) | 2 | 2 |
| **OC6** | O | 0 | 0 | 0.117979 | 0.942(18) | 4 | 2 |

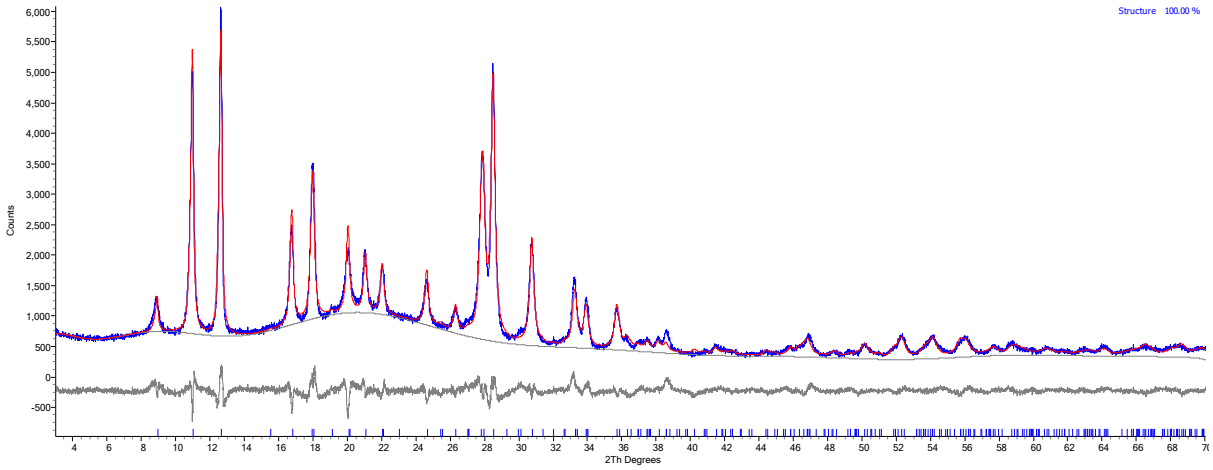


Figure S6.4. Rietveld plot of K,H-MER (536 mbar $CO_2$)

Table S6.5. Refined structure of K,H-MER (536 mbar $CO_2$)

| Site | Type | x | y | z | Occ | Mult | Biso |
|---|---|---|---|---|---|---|---|
| **K1** | K | 0 | 1 | 0.7650(17) | 0.418(16) | 4 | 2 |
| **K2** | K | 0.5 | 0.8128(7) | 1 | 0.538(6) | 8 | 2 |
| **K3** | K | 0 | 0.5 | 0.795(6) | 0.247(8) | 4 | 2 |
| **O1** | O | 0.1442(11) | 0.1645(10) | 0.1940(12) | 1 | 16 | 1 |
| **O2** | O | 0.1243(9) | 0.2845(8) | 0 | 1 | 16 | 1 |
| **O3** | O | 0 | 0.2827(17) | 0.209(2) | 1 | 8 | 1 |
| **O5** | O | 0.7916(14) | 0 | 0.188(2) | 1 | 8 | 1 |
| **O4** | O | 0.1765(11) | 0.3535(12) | 0.2370(13) | 1 | 16 | 1 |
| **Si1** | Si | 0.1141(6) | 0.2712(5) | 0.1646(10) | 0.8 | 16 | 1 |
| **Al1** | Al | 0.1141(6) | 0.2712(5) | 0.1646(10) | 0.2 | 16 | 1 |
| **Si2** | Si | 0.7579(5) | 0.1079(6) | 0.1604(10) | 0.8 | 16 | 1 |
| **Al2** | Al | 0.7579(5) | 0.1079(6) | 0.1604(10) | 0.2 | 16 | 1 |
| **C1** | C | 0.5 | 0.5 | 0 | 0.669(15) | 2 | 2 |
| **OC1** | O | 0.5 | 0.5 | 0.117948 | 0.669(15) | 4 | 2 |
| **C2** | C | 0.1845(14) | 0 | 0.5 | 0.287(6) | 8 | 2 |
| **OC2** | O | 0.1845(14) | -0.08292 | 0.5 | 0.287(6) | 16 | 2 |
| **C6** | C | 0 | 0 | 0 | 0.911(17) | 2 | 2 |
| **OC6** | O | 0 | 0 | 0.117948 | 0.911(17) | 4 | 2 |

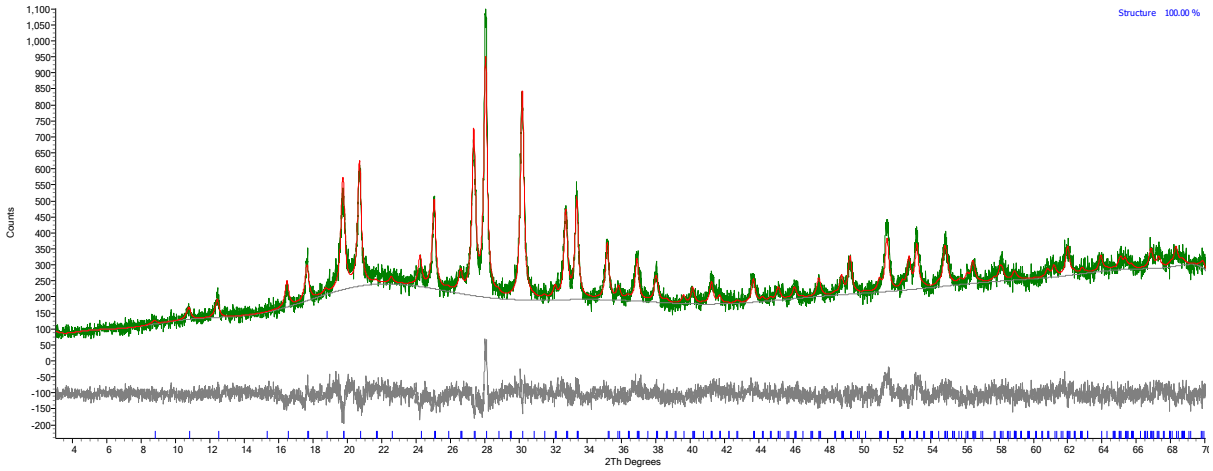


Figure S6.5. Rietveld plot of Cs-MER (500 mbar $CO_2$)

Table S6.6. Refined structure of Cs-MER (500 mbar $CO_2$)

| Site | Type | x | y | z | Occ | Mult | Biso |
|---|---|---|---|---|---|---|---|
| **Cs1** | Cs | 0 | 1 | 0.7271(11) | 0.530(8) | 4 | 2 |
| **Cs2** | Cs | 0.5 | 0.8081(6) | 1 | 0.443(4) | 8 | 2 |
| **Cs3** | Cs | 0 | 0.5 | 0.681(3) | 0.253(6) | 4 | 2 |
| **O1** | O | 0.161(6) | 0.160(6) | 0.183(2) | 1 | 16 | 1 |
| **O2** | O | 0.1220(16) | 0.2917(14) | 0 | 1 | 16 | 1 |
| **O3** | O | 0 | 0.251(7) | 0.196(8) | 1 | 8 | 1 |
| **O5** | O | 0.748(7) | 0 | 0.196(8) | 1 | 8 | 1 |
| **O4** | O | 0.16(4) | 0.34(4) | 0.250(7) | 1 | 16 | 1 |
| **Si1** | Si | 0.112(3) | 0.259(4) | 0.157(2) | 0.8 | 16 | 1 |
| **A11** | Al | 0.112(3) | 0.259(4) | 0.157(2) | 0.2 | 16 | 1 |
| **Si2** | Si | 0.740(4) | 0.111(3) | 0.155(2) | 0.8 | 16 | 1 |
| **A12** | Al | 0.740(4) | 0.111(3) | 0.155(2) | 0.2 | 16 | 1 |
| **C1** | C | 0.5 | 0.5 | 0 | 0.28(4) | 2 | 2 |
| **OC1** | O | 0.5 | 0.5 | 0.115812 | 0.28(4) | 4 | 2 |
| **C2** | C | 0.1659(19) | 0 | 0.5 | 0.467(14) | 8 | 2 |
| **OC2** | O | 0.1659(19) | -0.08171 | 0.5 | 0.467(14) | 16 | 2 |
| **C3** | C | 0 | 0.5 | 0 | 0.49(3) | 4 | 2 |
| **OC3** | O | 0.081707 | 0.5 | 0 | 0.49(3) | 8 | 2 |
| **C6** | C | 0 | 0 | 0 | 0.50(3) | 2 | 2 |
| **OC6** | O | 0 | 0 | 0.115812 | 0.50(3) | 4 | 2 |

## S7. Single component $CO_2$ and $CH_4$ isotherms and $CO_2/CH_4$ breakthrough curves

### Single Component $CH_4$ and $CO_2$ Isotherm Measurement

$CH_4$ adsorption isotherms (and comparative $CO_2$ isotherms) for K,H-MER, Na-MER, and Cs-MER were measured volumetrically (see SI for details). using a 3FLEX Surface Characterization Unit from Micromeritics for pressures measured up to 800 Torr (1.07 bar) absolute at 298 K. Comparative $CO_2$ isotherms were also measured on this unit. Each sample port on the 3FLEX unit is equipped with a 0 – 10 torr and 0-1000 torr pressure transducer with +/- 0.12% and 0.15% accuracy, respectively. A turbomolecular pump in combination with a roughing pump were used for out gassing samples prior to analysis. The samples had been heated to 363 K at 2 K $min^{-1}$ under vacuum and held for one hour, before being heated to 498 K (or 523 K for Cs-MER) under vacuum at 2 K $min^{-1}$ and held at this temperature for 12 h before cooling and measurement. Sample weights ranging from 0.2257 g to 0.4217 g were loaded into 12 mm quartz tubes under a nitrogen atmosphere. The samples were then further degassed on the 3FLEX at 383 K for 3-4 hours to a final pressure of $10^{-4}$ to $10^{-5}$ torr. A recirculating bath was equilibrated to 298 K, and a warm and cold free space are measured on the 3Flex to determine the void volume of the sample + tube. The pressure tables for $CH_4$ (Airgas 99.999%) and $CO_2$ (Airgas Instrument Grade) spanned from 0.5 torr to 800 torr with a total of 19 equilibrated points taken. An absolute pressure dosing method was used with 60 second equilibration intervals at each pressure point. Once the rate of change at each point was <0.01% over the interval, the mmol $g^{-1}$ adsorbed at the equilibration point is calculated and the isotherm continues to the next pressure set point.

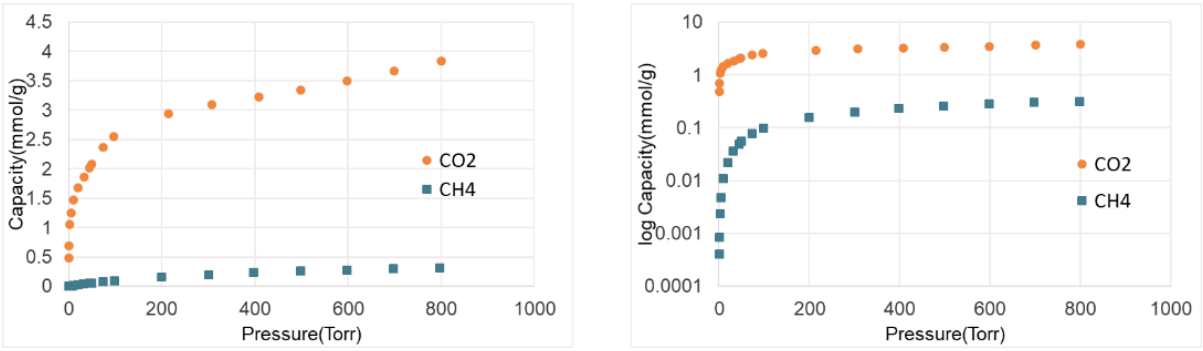


Figure S7.1. $CO_2$ and $CH_4$ isotherms on Na-MER at 303 K

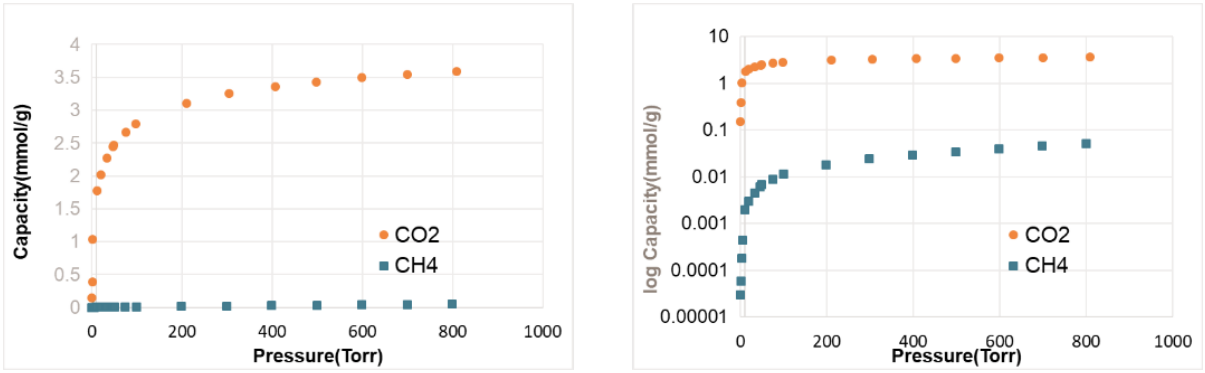


Figure S7.2. $CO_2$ and $CH_4$ isotherms on K-MER at 298 K

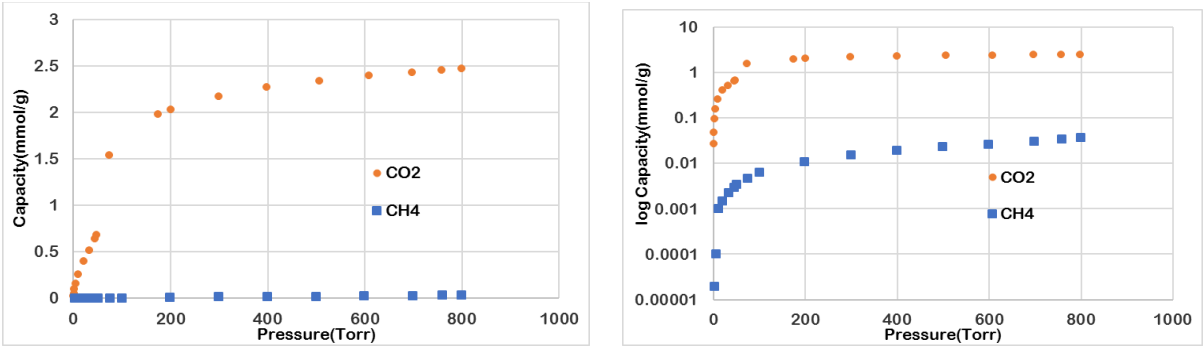


Figure S7.3. $CO_2$ and $CH_4$ isotherms on Cs-MER at 298 K

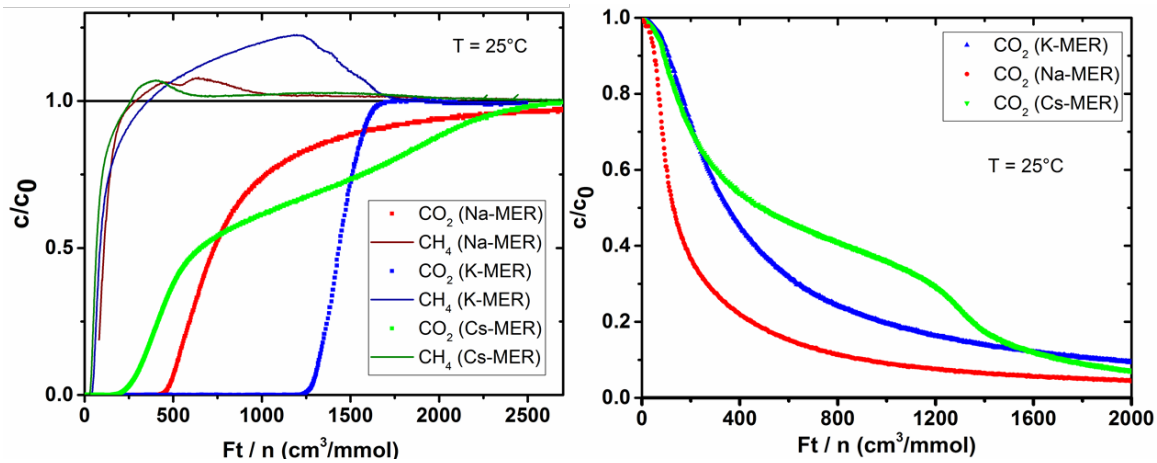


Figure S7.4. Comparison of breakthrough curves of $CO_2/CH_4$/He 10:40:50 mixtures and desorption curves of $CO_2$ over Na-, K- and Cs-MER.

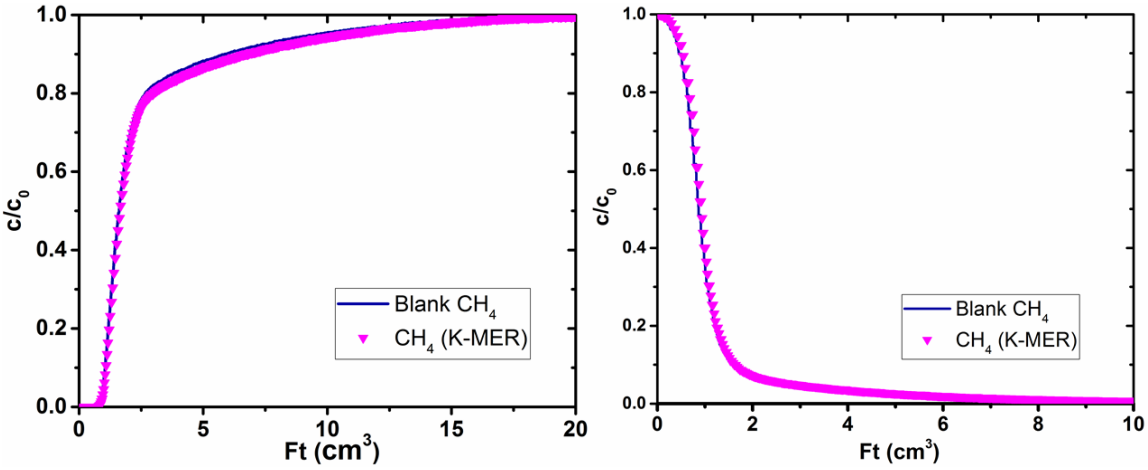


Figure S7.5. Breakthrough curve (left: adsorption; right: desorption) for K-MER in 40% $CH_4$ / 60% He at 298 K. The curves are shown as a function of eluted volume of gas.

**Table S7.1 Uptakes after Mixed Component Adsorption Experiments at 298 K**

| Sample | $p_{CH4}$ / bar | $p_{CO2}$ / bar | $CH_4$ uptake / mmol $g^{-1}$ | $CO_2$ uptake / mmol $g^{-1}$ | Selectivity $CO_2/CH_4$ |
|---|---|---|---|---|---|
| Na-MER | 0.4 | 0.1 | 0.0170 | 1.242 | 292 |
| Na-MER (rpt) | 0.4 | 0.1 | 0.0141 | 1.106 | 314 |
| K-MER | 0.4 | 0.1 | 0.0090 | 1.912 | 850 |
| Cs-MER | 0.4 | 0.1 | 0.0136 | 1.157 | 340 |

## S8. Kinetic measurements using the Zero Length Column technique

The Zero Length Column (ZLC) technique has been described in detail in references 7 and 8. Figure S8.1 shows the normalised desorption data for Na-MER in 1% $CO_2$ in helium at ambient pressure (i.e. $p_{CO2}$ = 0.01 bar) and at T = 308 K versus eluted volume from the column. The data at different flow rates does not overlap, which indicates kinetic control. Figures S8.2 show the normalised desorption data versus time, but now with fits using the analytical solution given in equations 1 – 4. This equation assumes a linear isotherm, but Brandani has shown that the using equation to estimate the diffusional time constants for Langmuir isotherms with amounts adsorbed up to $q/q_s = 0.5$ (where $q_s$ is the saturation capacity) would result in relatively small errors.[9] Figures S8.2 show that indeed the model fits the data well, indicating Langmuir type behaviour for Na-MER under these conditions with no signs of structural changes. A partial loading experiment is also reproduced well by the analytical solution, also seen in Figure S8.2. The values for L > 10 also confirms kinetic control, which is an additional check to justify carrying out kinetic analysis. Performing the experiments at different temperatures yields an activation energy for the diffusivity, $D/R^2$, of 18 kJ $mol^{-1}$ (Figure S8.3). This allows calculation of the diffusivity at T = 298 K, i.e. $D/R^2$ (298 K) = 2.0 × $10^{-4}$ $s^{-1}$.

| | |
|---|---|
| $\frac{c}{c_0} = 2L\sum_{n=1}^{\infty}\frac{\exp\left(-\beta_n^2 Dt/R^2\right)}{\beta_n^2 + (1-L+\gamma\beta_n^2)^2 + L - 1 + \gamma\beta_n^2}$ | 1 |
| $\beta_n cot\beta_n + L - 1 - \gamma\beta_n^2 = 0$ | 2 |
| $L = \frac{1}{3}\frac{F}{KV_s}\frac{R^2}{D}$ | 3 |
| $\gamma = \frac{1}{3}\frac{V_f}{KV_s}$ | 4 |

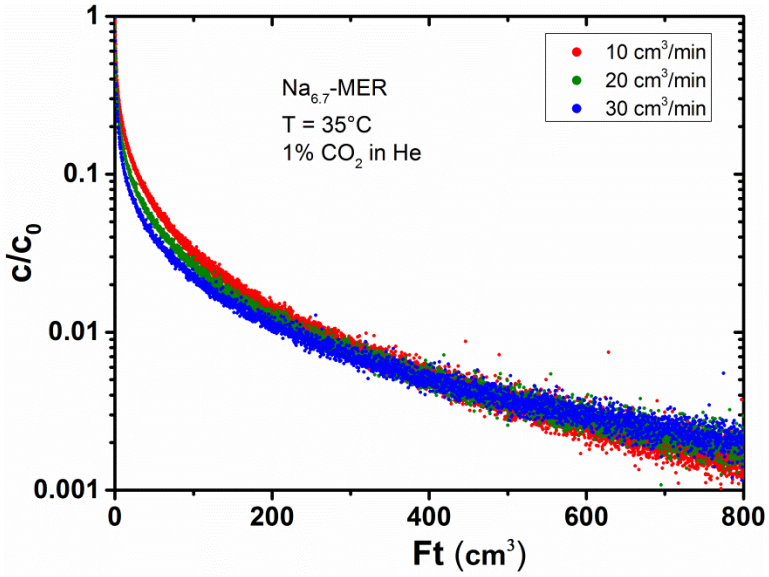


Figure S8.1. Normalised concentration $c/c_0$ vs. eluted volume for Na-MER. The lack of overlap indicates kinetic control and justifies carrying out kinetic analysis.

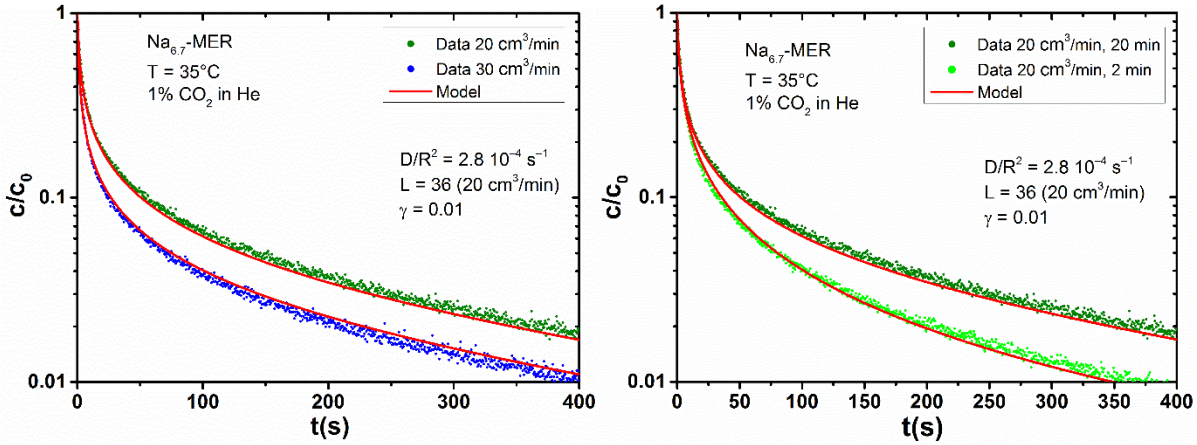


Figure S8.2. Normalised concentration $c/c_0$ vs. time for Na-MER including fits according to the analytic model as given by equations 1 – 4 (left). A partial loading experiment (right) can be fitted using identical fitting parameters.

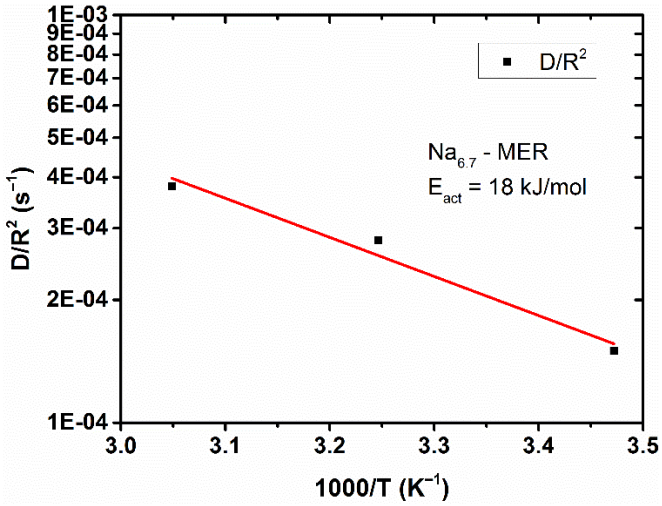


Figure S8.3. Diffusivity values for Na-MER at different temperatures allows for an estimation of its activation energy.

The normalised concentration versus time plot for K-MER in 10% $CO_2$ in He at ambient pressure and T = 298 K is shown in Figure S8.4. It also includes desorption from a blank column (i.e. without adsorbent). The curves for the different flow rates were found to be overlapping in the plots of $c/c_0$ vs. eluted volume for the initial part of the desorption (down to $pCO_2 \sim 0.003$ bar), after which the curves start deviating. This is believed to be due to the transition from large pore to narrow pore phase. It indicates that the large pore phase has fast kinetics and remains under equilibrium control, whereas $CO_2$ desorption in the narrow pore phase is kinetically controlled under these conditions. Since at these low concentrations we cannot neglect the kinetics of the experimental setup (the mass spectrometer has a particularly large effect on the obtained data), we have performed the mathematical procedure of deconvolution to obtain the gas phase concentration coming out of the column. These deconvoluted data sets are shown in Figure S8.5. The long-time asymptote can be used to obtain kinetic information from the deconvoluted data (Figure 8.6). The slope can be approximated by equation 5, yielding $D/R^2$ of $2.5 \times 10^{-4}$ $s^{-1}$ at 298 K.

| | |
|---|---|
| $\frac{2}{L}\exp\left(-\beta_1^2 Dt/R^2\right)$ | 5 |

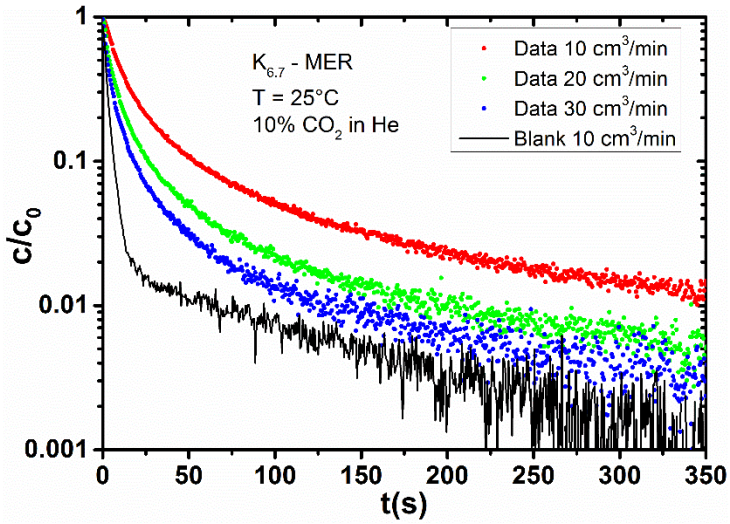


Figure S8.4. Normalised concentration $c/c_0$ vs. time for $K_{6.7}$-MER

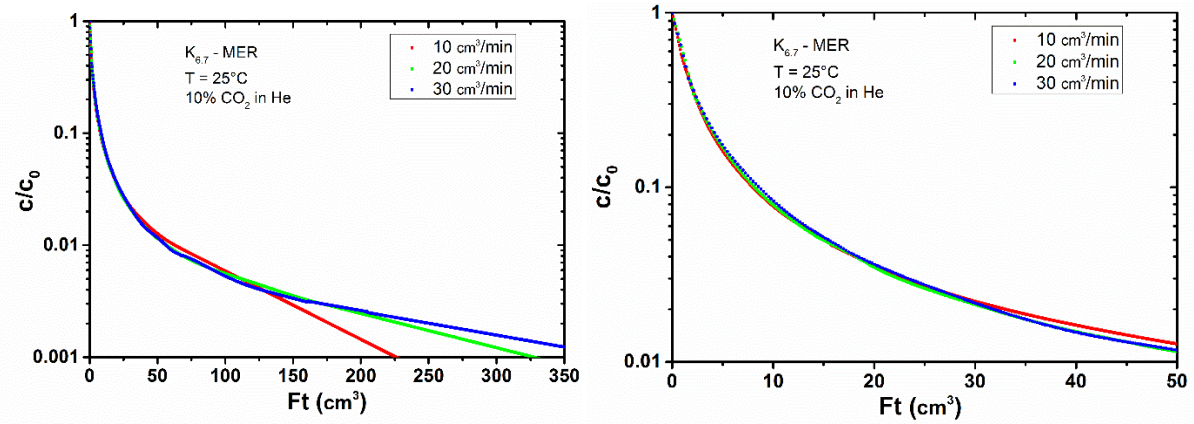


Figure S8.5. Normalised concentration $c/c_0$ obtained by deconvolution vs. eluted volume for $K_{6.7}$-MER. Curves overlap at initial stage of desorption, down to $c/c_0 \sim 0.03$, below which curves start to deviate.

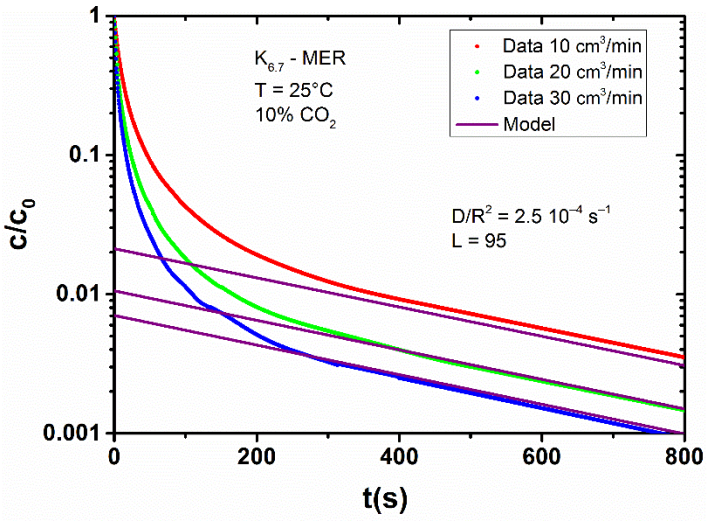


Figure S8.6. Normalised concentration $c/c_0$ as obtained by deconvolution vs. time for K-MER including long time asymptote fit (equation 5). The L values scale with flow rate as expected.

A similar procedure was used for Cs-MER. The plot of $c/c_0$ versus eluted volume in 10% $CO_2$ at ambient pressure at T = 298 K once more shows kinetic control (Fig. S8.7). The slope of the long time asymptote suggests a diffusivity in the narrow pore phase of $D/R^2 = 9 \times 10^{-4}$ $s^{-1}$ at 298 K.

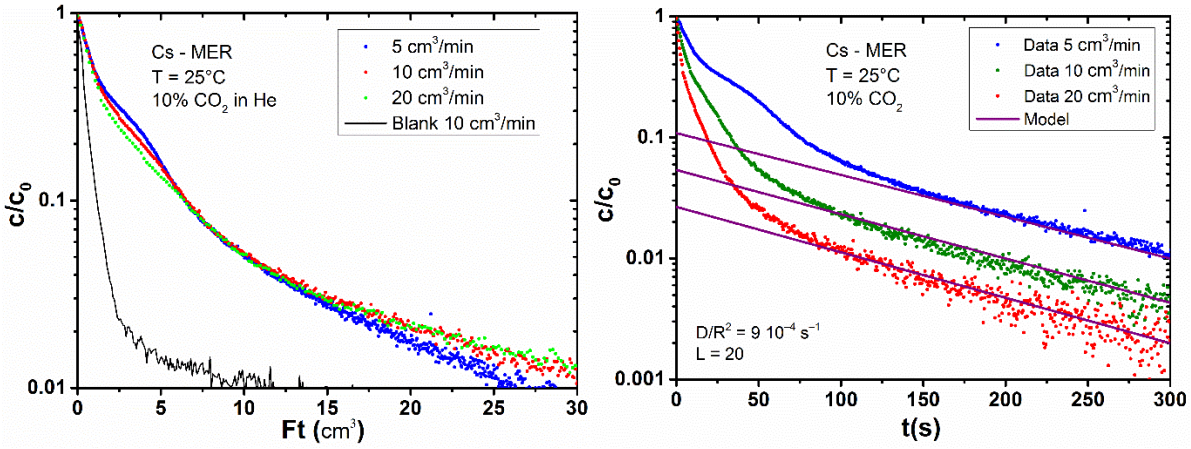


Figure S8.7. Normalised concentration $c/c_0$ vs. eluted volume for Cs-MER (left). The lack of overlap indicates kinetic control and justifies carrying out kinetic analysis. Normalised concentration $c/c_0$ as obtained by deconvolution vs. time for Cs-MER including long time asymptote fit (equation 5). The L values scale with flow rate as expected.

**S9. Summary of structural and adsorption studies on K, H-MER zeolite**

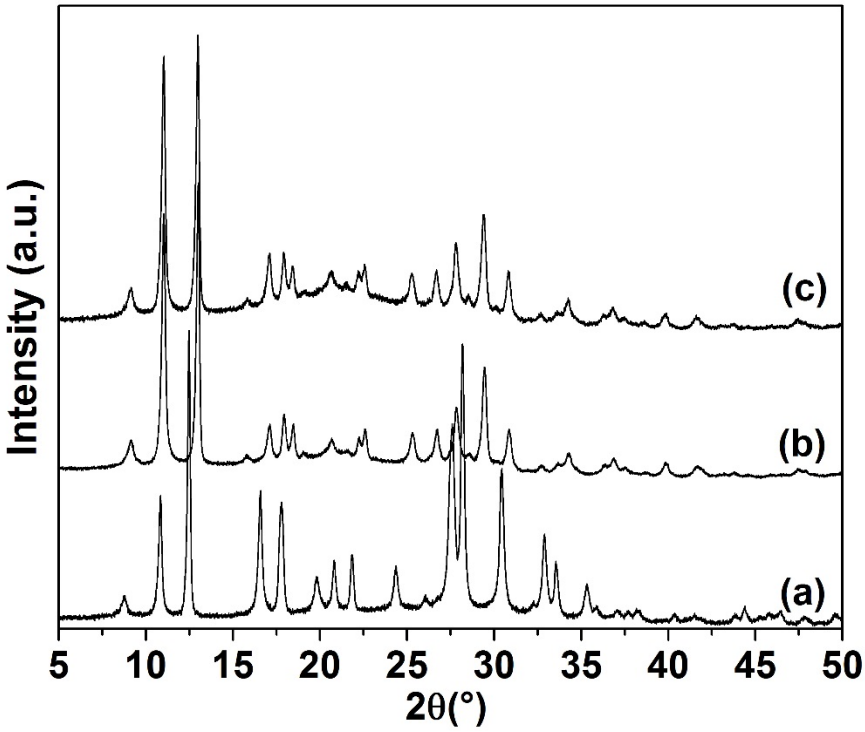


Figure S9.1. Capillary PXRD patterns of K,H-MER which was (a) hydrated, (b) dehydrated and flame sealed, (c) dehydrated and epoxy-sealed.

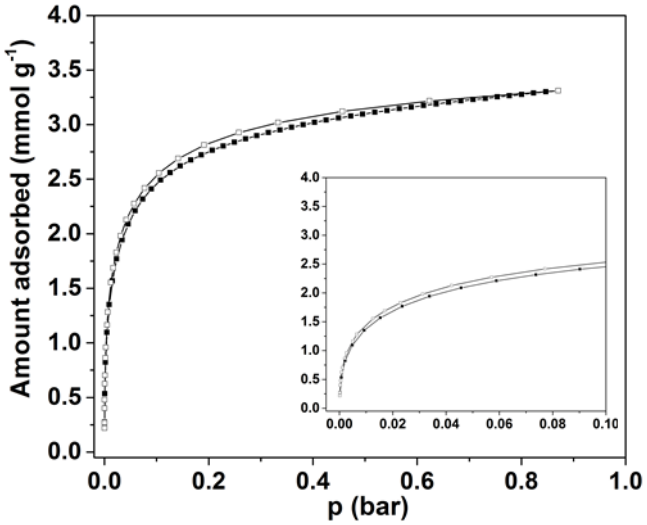


Figure S9.2. $CO_2$ isotherms up to 1 bar at 298 K for K,H-MER. Adsorption, closed symbols; desorption, open symbols. Inserts: lower pressures isotherm region (up to 0.1 bar).

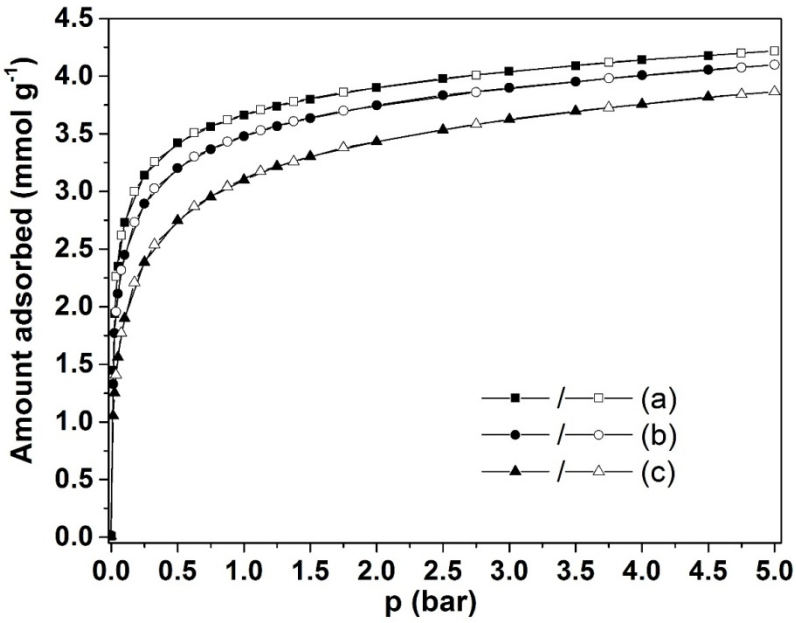


Figure S9.3. High pressure $CO_2$ isotherms at (a) 298 K, (b) 308 K and (c) 328 K for K,H-MER. Adsorption, closed symbols; desorption, open symbols.

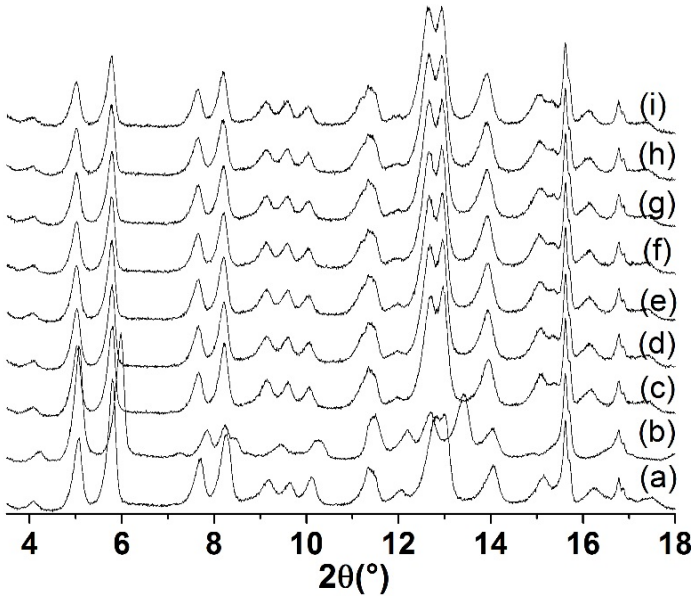


Figure S9.4. PXRD of K,H-MER where (a) hydrated, (b) dehydrated and measured with $CO_2$ adsorbed at 298 K at different pressures (in bar): (c) 0.1, (d) 0.2, (e) 0.3, (f) 0.4, (g) 0.6, (h) 0.8, (i) 1.

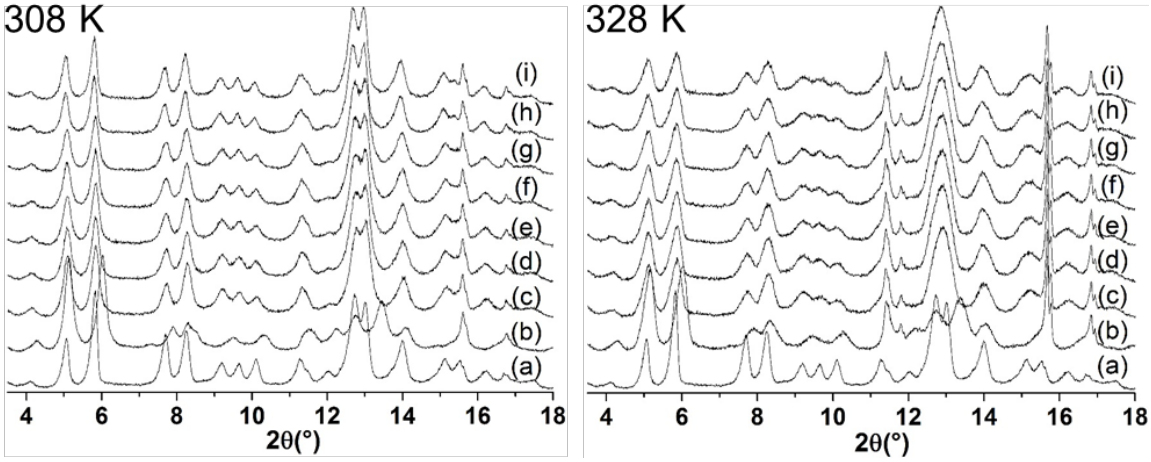


Figure S9.5. PXRD of K,H-MER where (a) hydrated, (b) dehydrated and measured with $CO_2$ adsorbed at different temperatures at different pressures (in bar): (c) 0.1, (d) 0.2, (e) 0.3, (f) 0.4, (g) 0.6, (h) 0.8, (i) 1.

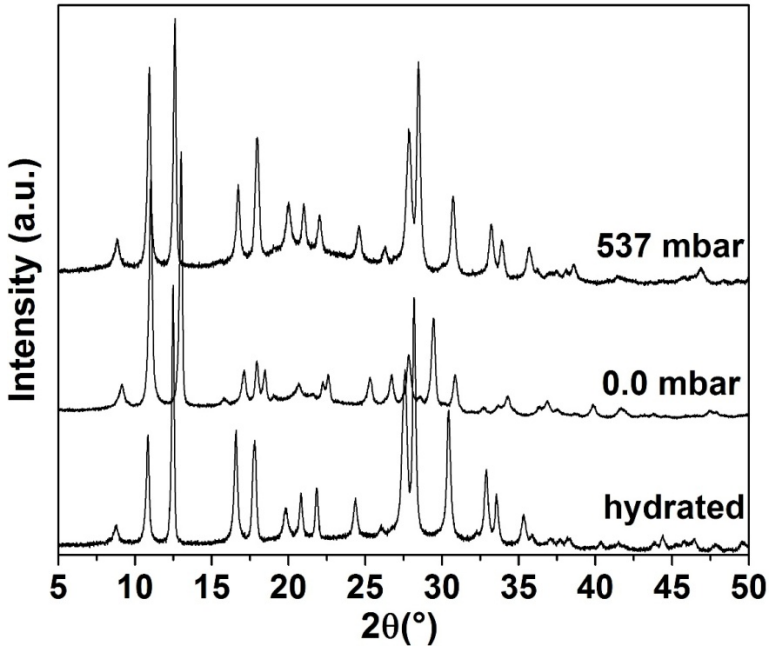


Figure S9.6. Capillary PXRD of (b) K,H-MER with $CO_2$ at different pressures.

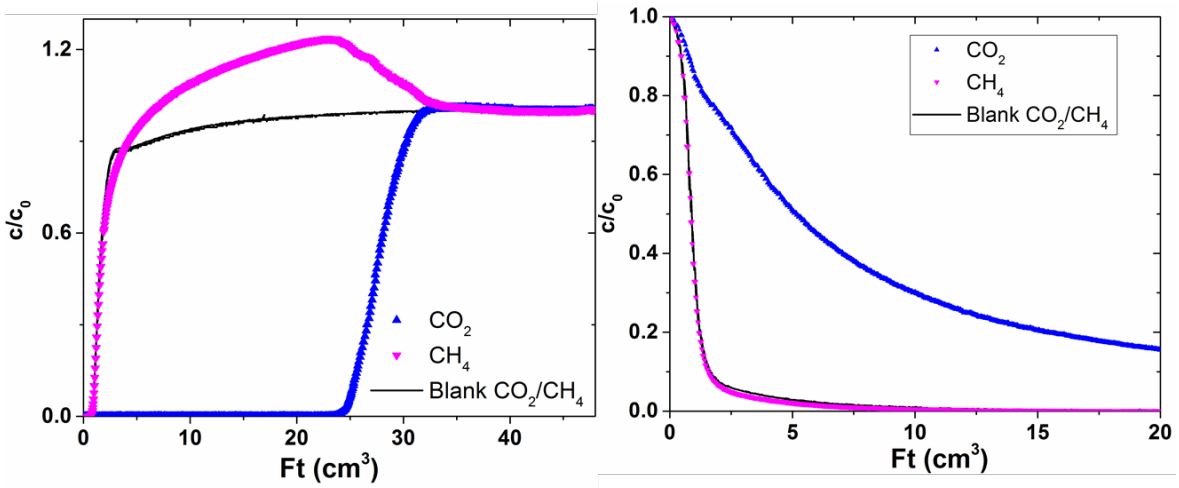


Figure S9.7. Breakthrough curve (left: adsorption; right: desorption) for K,H-MER in 40% $CH_4$ / 10% $CO_2$ / 50% He at 298 K. The curves are shown as a function of eluted volume of gas.

**References**


(1) Galli E.; Gottardi G.; Pongiluppi D. The crystal structure of the zeolite merlinoite, *Neues Jahrbuch für Mineralogie, Monatshefte* **1979**, 1-9

(2) Skofteland, B. M.; Ellestad, O. H.; Lillerud, K. P. Potassium merlinoite: Crystallization, structural and thermal properties. *Microporous Mesoporous Mater.* **2001,** *43*, 61–71.

(3) Pakhomova, A. S.; Armbruster, T.; Krivovichev, S. V.; Yakovenchuk, V. N. Dehydration of the zeolite merlinoite from the Khibiny massif, Russia: an *in situ* temperature-dependent single-crystal X-ray study. *Eur. J. Mineral.* **2014***, 26*, 371–380.

(4) Bieniok, A.; Bornholdt, K.; Brendel, U.; Baur, W. H. Synthesis and crystal structure of zeolite W, resembling the mineral merlinoite. *J. Mater. Chem.* **1996,** *6*, 271–275.

(5) Barrett, P. A.; Valencia, S.; Camblor, M. A. Synthesis of a merlinoite-type zeolite with an enhanced Si/Al ratio via pore filling with tetraethylammonium cations, *J. Mater. Chem.* **1998,** *8*, 2263–2268.

(6) Yakubovich, O.V.; Pekov, I.V.; Kucherinenko, Ya.V.; Massa, W. Crystal structure of a Na,K-variety of merlinoite. *Crystallography Reports* **1999***, 44(5)*, 776-782.

(7) Eic, M.; Ruthven, D. M. A new experimental technique for measurement of intracrystalline diffusivity. *Zeolites* **1988***, 8*, 40–45.

(8) Brandani, S.; Ruthven, D. M. Analysis of ZLC desorption curves for liquid systems. *Chem. Eng. Sci.* **1995** *50*, 2055–2059.

(9) Brandani, S.; Jama, M. A.; Ruthven, D. M. ZLC Measurements under non-linear conditions. *Chem. Eng. Sci.* **2000** *55*, 1205–1212.